8-2012

Optimal Energy Management for Microgrids

Zheng Zhao
Clemson University, zzhao@clemson.edu

Optimal Energy Management for Microgrids

A Dissertation
Presented to
the Graduate School of
Clemson University

In Partial Fulfillment
of the Requirements for the Degree
Doctor of Philosophy
Electrical and Computer Engineering

---

by
Zheng Zhao
August 2012

Accepted by:
Dr. Elham Makram, Committee Chair
Dr. Kumar Venayagamoorthy
Dr. Timothy Burg
Dr. Richard Groff
Dr. Pietro Belotti

ABSTRACT

Microgrid is a recent novel concept in part of the development of smart grid. A microgrid is a low voltage and small scale network containing both distributed energy resources (DERs) and load demands. Clean energy is encouraged to be used in a microgrid for economic and sustainable reasons. A microgrid can have two operational modes, the stand-alone mode and grid-connected mode. In this research, a day-ahead optimal energy management for a microgrid under both operational modes is studied. The objective of the optimization model is to minimize fuel cost, improve energy utilization efficiency and reduce gas emissions by scheduling generations of DERs in each hour on the next day. Considering the dynamic performance of battery as Energy Storage System (ESS), the model is featured as a multi-objectives and multi-parametric programming constrained by dynamic programming, which is proposed to be solved by using the Advanced Dynamic Programming (ADP) method. Then, factors influencing the battery life are studied and included in the model in order to obtain an optimal usage pattern of battery and reduce the correlated cost. Moreover, since wind and solar generation is a stochastic process affected by weather changes, the proposed optimization model is performed hourly to track the weather changes. Simulation results are compared with the day-ahead energy management model. At last, conclusions are presented and future research in microgrid energy management is discussed.

.

DEDICATION

I would like to dedicate this thesis to my family, my dear mother and father, for all of their love and support; to my girlfriend, Haiqin Dong, for her great encouragement and tender care.

ACKNOWLEDGMENTS

I would like to thank my major advisor, Dr. Elham Makram, for all her kindly help and guidance. I have learned so much from her. Also, I would like to thank my committee members, Dr. Kumar Venayagamoorthy, Dr. Timothy Burg, Dr. Richard Groff and Dr. Pietro Belotti, for their kindly suggestions and great patience.

TABLE OF CONTENTS

Page

TABLE OF CONTENTS (continued)

Page

LIST OF TABLES

LIST OF FIGURES

List of Figures (Continued)

List of Figures (Continued)

Figure Page

LIST OF ABBREVIATIONS

PV ----- Photovoltaic

WT ----- Wind Turbine

MT ----- Microturbine

FC ----- Fuel Cell

DG ----- Distributed Generator

ESS ----- Energy Storage System

DER ----- Distributed Energy Resource

DFIG ----- Doubly-Fed Induction Generator

SFIG ----- Single-Fed Induction Generator

PMSG ----- Permanent Magnet Synchronous Generator

ADP ----- Advanced Dynamic Programming

MSDP ----- Multi-Stage Decision Process

SQP ----- Sequential Quadratic Programming

PCC ----- Point of Common Coupling

MPPT ----- Maximum Power Point Tracking

EMS ----- Energy Management System

CHAPTER ONE

INTRODUCTION

1.1 Background of microgrid

With the increased use of renewable energy resources, substantial efforts have been invested in the installation of distributed energy resources (DERs) for establishing a green and smart distribution system. Generally, DERs include diverse technologies, such as diesel generator, fuel cell, microturbine, and energy storage system (ESS) belonging to controllable energy resources, as well as wind energy and photovoltaic as non-controllable renewable energy resources. According to the US Department of Energy [1], relying on the advanced communication tools and power electronic control devices, the utilization of DERs is potentially in favor of increasing the energy utilization efficiency, mitigating the power flow congestion in distribution system, improving the system stability and reliability, providing more benefits in both economic and sustainability reasons, and strengthening the centralized control for grid operation.

Even if DERs have many advantages, they also bring problems to the power network. A single and small DER is treated as a non-regulated energy resource compared to the large power grid. The integration of DERs into power grid causes voltage fluctuations and affects power quality. Moreover, DERs need to be disconnected instantly if severe faults occur in the main grid. It may limit the performance of DERs to a large extent. To obtain a better and stable use of DERs and release the conflicts between a single DER and large power network, a new concept called “Microgrid” has been developed in recent years.

Microgrid is an important and necessary part of the development of smart grid, and found to possess much practicability in a smart grid [2]. A microgrid is a low-voltage and small network connected to a distribution grid through the point of common coupling (PCC), and contains both distributed generations and loads. Several types of distributed energy resources (DERs) are used in a microgrid, such as microturbine (MT), fuel cell (FC) and energy storage system (ESS) as controllable units. Renewable energy, such as wind energy and photovoltaic, are also included in a microgrid as non-controllable units.

Normally, a microgrid has two modes of operation: the stand-alone mode and the grid-connected mode. If a microgrid operates in a stand-alone mode, the power generation produced within the microgrid is required to satisfy its local load demand. While the microgrid works in a grid-connected mode, it can either send power to the main grid or receive power from the main grid. The operational mode of a microgrid is related to the local power generation production, the local load demands and the electricity price in the main grid. For a single renewable energy unit (wind or solar energy) without much reactive power compensation connected to a distribution network, it is normally forced to be disconnected from the distribution network if a severe fault occurs in the main grid, in order to avoid any further damage. In that case, a microgrid can be disconnected from the main grid and operates in a stand-alone mode. The DERs in the microgrid can operate in normal conditions without any damages. From this point of view, it is easy to see a more flexible operation feature of microgrids than the DERs connected directly to the main grid. Fig.1.1 shows a microgrid connected to the

distribution network through a PCC, and several types of DERs are included in this microgrid.

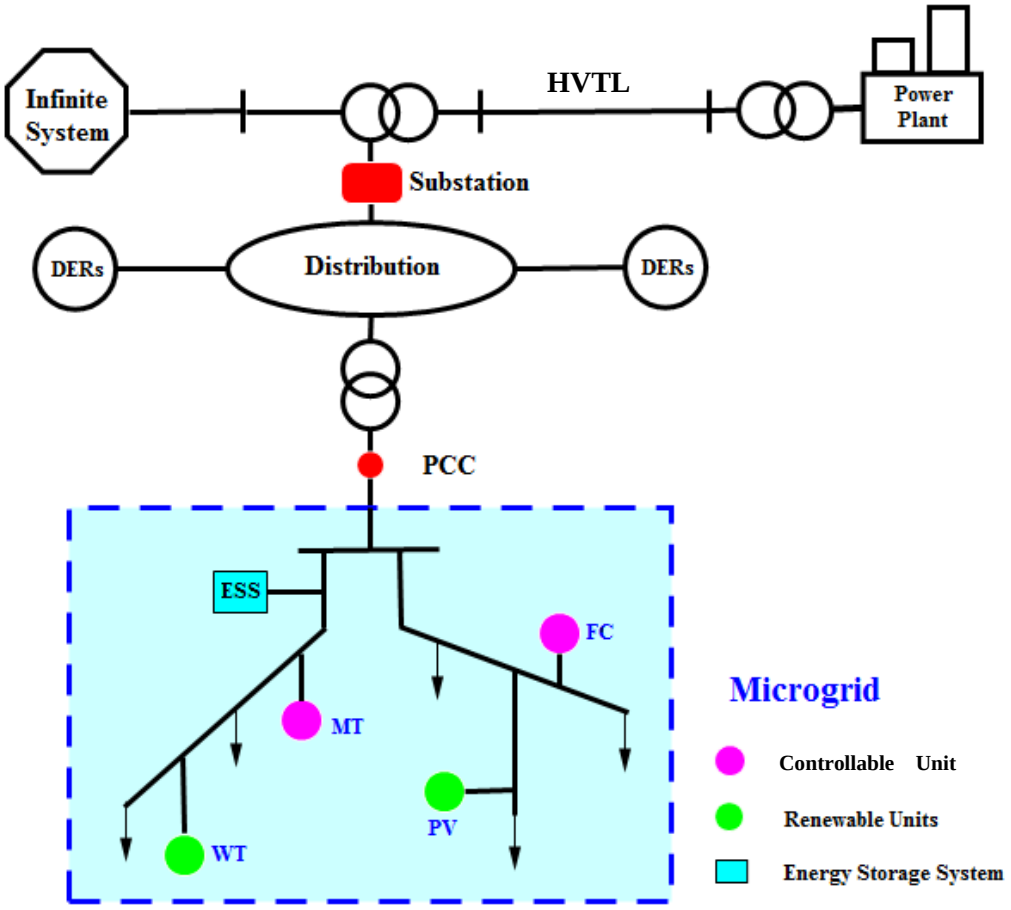

Fig. 1.1 A typical microgrid interconnected with the main grid.

In conclusion, the following benefits can be seen by building a microgrid:

- Sustainability -- Utilize renewable energy, reduce fuel cost and gas emissions;
- Flexibility -- Two operational modes, grid-connected and stand-alone mode;
- Reliability -- When a severe fault occurs in the main grid, a microgrid is able to isolate itself from the main grid.

1.2 Research Objectives

An Energy Management System (EMS) is a computer-aided tool used by power system operators to monitor, control, and carry out the optimal energy management. The purpose of EMS is to produce demanded power with least cost and least environmental effect.

In this research, the optimization model of EMS in a microgrid is to plan a generation schedule for each unit in each hour on the next day with the objectives shown below:

- Minimize the fuel cost.
- Minimize harmful gas emissions.
- Improve energy utilization efficiency.
- Maximize microgrid operation profits under different operational conditions.

These goals are subjected to the constraints that the total power supply should be equal to the load demands in each time interval and each DER unit should operate within its minimum and maximum limits. A time interval is normally set to 15 minutes, 30 minutes or 1 hour. Some information should be known in advance for a day-ahead energy management, such as the DER parameters, the forecasted wind and solar generation in each hour on the next day, the forecasted market electricity price on the next day and also the load demand forecasting. Then, the prepared data are sent to the EMS optimization engine as inputs. Finally, the outputs from the optimization engine show the best generation schedule for the next day. The generation schedules are able to guide power companies operating the power network inexpensively and efficiently.

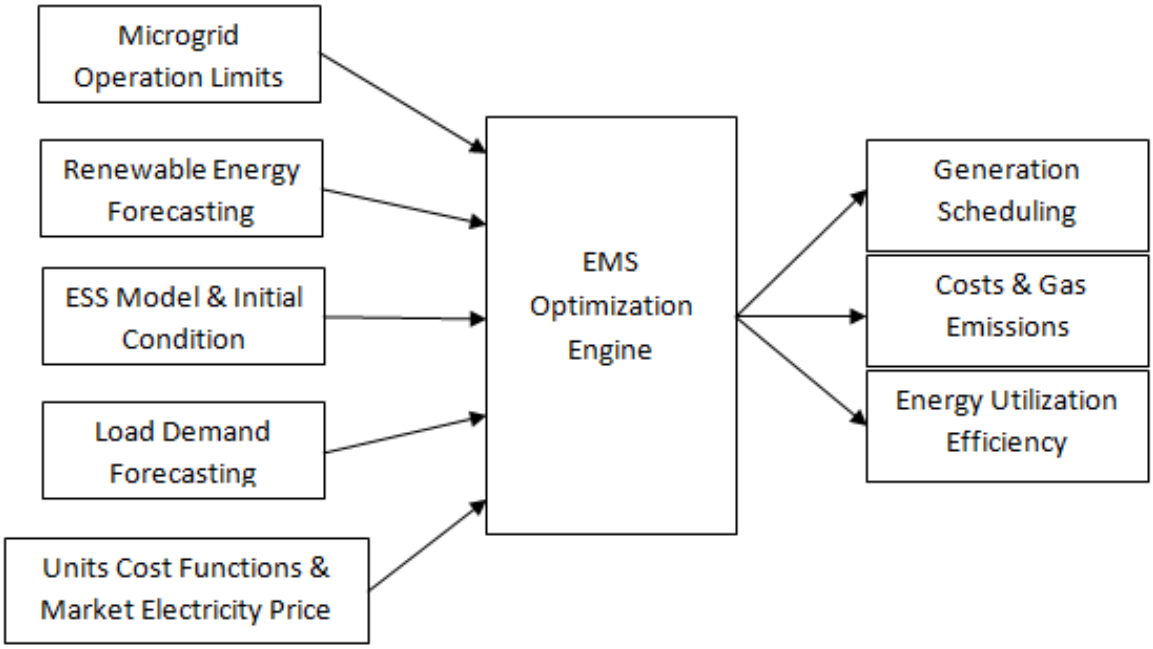

Fig. 1.2 EMS optimization in a microgrid

The major difference between the energy management in a conventional power grid and a microgrid is the algorithms used within the optimization engine. The following paragraphs describe the algorithm differences.

a) Conventional Energy Management

In a traditional day-ahead energy scheduling problem, one has the following basic information in advance, which includes the generators operational limits, the cost function of each generator, the forecasted loads on the following day, the forecasted wind generation and solar generation on the following day. The formulations for the optimal energy management can be simplified in equation (1.1):

Objective function

$$\Gamma = \Gamma(x,u,d) \tag{1.1}$$

Subjected to

$$c_E(x,u,d) = 0$$

$$c_I(x,u,d) \le 0\,,$$

where x is the state variables representing the active power output of all generators; u is the control variables such as the excitation current of a generator which can adjust the power output; d is the disturbance variables, such as the load changes or wind speed changes affecting wind turbines; Γ is the goal function minimizing the fuel cost, and the cost value is a function of state variables, control variables and disturbance variables; c_E is the equality constraint and c_I is the inequality constraint. The set of formulations is a multi-variables nonlinear programming. This problem can be resolved by some typical nonlinear programming methods, such as the Lagrange multiplier method, the interior-point method, the gradient projection method and so on. Some heuristic methods can also be applied to this problem, such as the genetic algorithm (GA) and particle swarm optimization (PSO).

b) Energy Management in a Microgrid

As clean energy is promoted in distribution grid and microgrid for building a green and sustainable environment, ESS gains more and more concentration than before due to its coordination with DERs, which can improve the energy utilization efficiency

and stabilize the system voltage and frequency. Among several types of ESS such as the flywheel, super capacitor, battery and so on, battery is the most used one due to its low cost and its convenience of installation and maintenance. A fact emerges in microgrid energy management model that the battery state of charge (SOC) in each hour depends on the SOC in the previous hour. Hence, the battery SOCs in each two adjacent hours are correlated and the optimization model is constrained by a dynamic programming. The simplified expression of the model is shown as follows.

Objective function

$$\Gamma = \Gamma(x,u,d) \tag{1.2}$$

Subjected to

$$c_E(x,u,d) = 0$$

$$c_I(x,u,d) \le 0$$

$$x_{i+1} = g(x_i, u_i, d_i),$$

where the last constraint indicates that the current state vector is a function of the state variables, control variables and disturbance variables in the previous interval. The system states in time interval i and $i+1$ are correlated. In this case, the model is determined as a multi-parametric nonlinear programming constrained by dynamic programming, which is hard to solve.

Various algorithms for the optimization of microgrid energy management were proposed [3-7]. In reference [3], the author clearly stated the model and cost function of each type of DER. GA-based algorithms and game theory are used to obtain the optimal

solution. An MRC-GA optimization module was proposed for search optimal generation schedule in reference [4] and particle swarm optimization (PSO) technique was implemented in references [5-6]. However, the heuristic methods can only approach, but not guarantee, the global optimal solution. Some of these methods rely on initial guesses to reach the best result and are time-consuming and inefficient. A modified dynamic programming method was considered in reference [7], but the author simplified the model by replacing some important stochastic variables with fixed values.

1.3 Contributions

Since the development of microgrid is still in an initial stage, technologies related to the optimal energy management in microgrid are not matured and numerous researchers have contributed diverse and valuable ideas. This research presents several contributions and it will be summarized as follows:

1) The dynamic performance of the battery is considered in this model and the advanced dynamic programming (ADP) method is used to solve the model featured as multi-parametric nonlinear programming constrained by dynamic programming. Previously, the model is simplified by limiting the performance of the battery, some researchers used heuristic algorithms to search the optimal solution which is slow and cannot guarantee the accuracy, while other references did not include the battery in their model. The ADP method was first proposed in 1999 by C. R. Dohrmann and R. D. Robinett [8], and later in 2005. This method was discussed in [9], and it is proved to have great results in the optimization of complex dynamic systems.

2) The consideration of battery life is included in the model in order to avoid an overuse of battery, extend the battery service life and thus reduce the cost spent on batteries. Previous research only included the capital cost of the battery, while other research optimized the performance of battery for the purpose of reducing fuel cost and satisfying the load demand but the battery life was neglected. In this research, both the objectives reducing cost and keeping an optimal usage pattern of the battery are considered in a model with assigned weighting factors.

3) The hourly energy management model is also implemented in this research by using ADP algorithm and considering the dynamic performance of battery. In previous research, the majority of the models work for day-ahead energy management and few discussed the hourly or real-time energy management in microgrid. The inclusion of wind generation or solar generation brings stochastic events into the model, so a day-ahead model may lose accuracy due to the external weather changes, whereas an hourly model could track the actual circumstances and reduce the errors between the scheduled generations and actual generations of DERs.

1.4 Thesis Outline

This thesis consists of six chapters. Chapter one introduces including the microgrid, the research objectives, and the contributions. Chapter two is about the models of typical DERs in microgrid, including the wind turbine, photovoltaic cell, microturbine, fuel cell and battery. Chapter three is the basic model for optimal energy management in microgrid, and the advanced dynamic programming method. The battery life is regarded as a factor and included into the basic model in chapter four. In chapter five, an hourly model is proposed to improve the accuracy of scheduling and track the external changes. In chapter six, the conclusion and future research are discussed.

CHAPTER TWO

DISTRIBUTED ENERGY RESOURCES IN MICROGRID

Before developing the model of optimal energy management in microgrid, it is necessary to get a general realization of the DERs used in microgrid. In the following sections, the fundamental models and related cost functions of typical DERs are introduced, which includes the wind turbine, photovoltaic cells (PV), microturbine, fuel cell and battery. These DERs is going to be used in the optimal energy management model in the following chapters.

2.1 Wind Turbines

Due to the advanced technology of wind turbines, wind generators are widely used as a clean energy source in power systems. In the following sections, three typical types of wind turbines in power industry are introduced. It includes the single-fed induction generator (SFIG), doubly-fed induction generator (DFIG) and permanent magnet synchronous generator (PMSG). Then, we discuss a comparison of the three types. Finally, the wind generation forecasting method is introduced.

1) SFIG

As shown in Figure 2.1, a SFIG consists of a wind rotor, a gear box, an induction generator, a capacitor bank and a transformer connected to the main grid. Firstly, wind drives the wind rotor with a low rotating speed. Then the gear box is used to increase the rotating speed and drives the rotor of the induction generator. The rotating magnetic field formed by the rotor dc excited current cuts the stator conductors and produces electricity.

The capacitor bank is connected to the grid side of the generator and compensates the SFIG with reactive power to keep the stator voltage stable. SFIG is a fixed speed wind turbine and has low generation capacity. If the wind speed is out of the rated speed, the SFIG is forced to cut off from the main grid in order to avoid any mechanical damage or poor generated power quality. The advantage of SFIG is that it has a low cost, small volume and is easy to install.

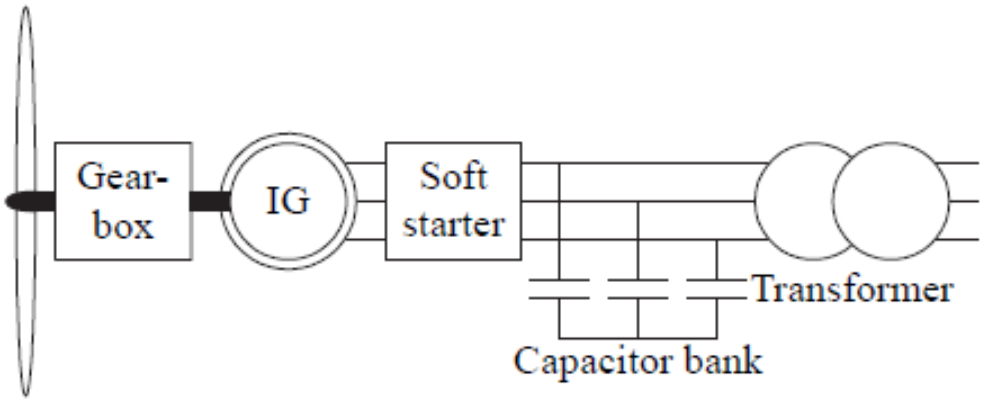

Fig. 2.1 Structure of SFIG

The P, Q generation of SFIG depends on the wind speed and cannot be adjusted separately. Integration of a group of SFIGs into the main grid induces voltage fluctuation and affects the power quality. Due to the low stability and reliability of SFIG, less and less SFIGs are used as wind generator units.

2) DFIG

DFIG is the most popular wind turbine used in current power industry due to its medium cost, high generation capacity and variable operational speed. Unlike SFIG,

there are two power flow paths linking the wind turbine and the main grid. The stator is directly connected to the grid and the rotor is also connected to the main grid through a power electronic converter. This converter is also called “back to back converter”, which consists of a rotor-side converter (RSC), a dc capacitor bank and a grid-side converter (GSC). The GSC is feed by the grid side ac voltage and functioned to maintain the voltage of dc link as a constant value. The RSC is controlled to provide the rotor with a desired AC excited current and keeps the stator current frequency the same as the system frequency. Normally, the converter handles around 30% power flow between the wind turbine and main grid.

Equation (2.1) explains the operation principle of a DFIG:

$$f_s = \frac{p}{60} n \pm f_r \ , \tag{2.1}$$

where

f_s : Stator current frequency, normally 60 Hz;

p : Pole pairs in the induction generator;

n : Rotor rotating speed, unit is r/min, the rotating speed depends on the wind speed;

f_r : Rotor current frequency; the rotor current is supplied by the RSC.

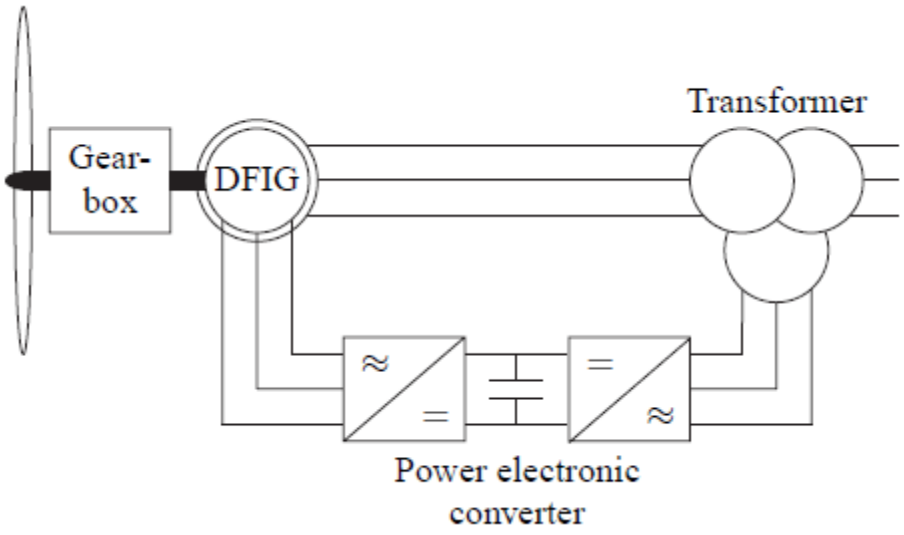

Fig. 2.2 Structure of DFIG

By using space vector control scheme [10-11], the P, Q generation of a DFIG can be adjusted separately. Space vector control is the most popular technique used in AC induction generator control. The explanation of vector control starts from the basic model of an induction generator. In the a-b-c three phase coordinate system, the induction generator can be modeled by,

$$\begin{bmatrix} u_{sa} \\ u_{sb} \\ u_{sc} \\ u_{ra} \\ u_{rb} \\ u_{rc} \end{bmatrix} = \begin{bmatrix} R_s & 0 & 0 & 0 & 0 & 0 \\ 0 & R_s & 0 & 0 & 0 & 0 \\ 0 & 0 & R_s & 0 & 0 & 0 \\ 0 & 0 & 0 & R_r & 0 & 0 \\ 0 & 0 & 0 & 0 & R_r & 0 \\ 0 & 0 & 0 & 0 & 0 & R_r \end{bmatrix} \begin{bmatrix} i_{sa} \\ i_{sb} \\ i_{sc} \\ i_{ra} \\ i_{rb} \\ i_{rc} \end{bmatrix} + \begin{bmatrix} \varphi_{sa} \\ \varphi_{sb} \\ \varphi_{sc} \\ \varphi_{ra} \\ \varphi_{rb} \\ \varphi_{rc} \end{bmatrix}. \tag{2.2}$$

In this equation,

u_{sa} , u_{sb} , u_{sc} , u_{ra} , u_{rb} , u_{rc} : Stator a-b-c phases voltages and rotor a-b-c phases voltages;

R_s , R_r : Stator and rotor resistances;

i_{sa} , i_{sb} , i_{sc} , i_{ra} , i_{rb} , i_{rc} : Stator a-b-c phases voltages and rotor a-b-c phases currents;

φ_{sa} , φ_{sb} , φ_{sc} , φ_{ra} , φ_{rb} , φ_{rc} : Stator a-b-c phases voltages and rotor a-b-c phases flux linkage;

The expression of stator and rotor flux linkages is shown in equation (2.3),

$$\begin{bmatrix} \varphi_{sa} \\ \varphi_{sb} \\ \varphi_{sc} \\ \varphi_{ra} \\ \varphi_{rb} \\ \varphi_{rc} \end{bmatrix} = \begin{bmatrix} L_{ms}+L_{ls} & -\frac{1}{2}L_{ms} & -\frac{1}{2}L_{ms} & L_{ms}\cos(\theta) & L_{ms}\cos(\theta+\frac{2}{3}\pi) & L_{ms}\cos(\theta-\frac{2}{3}\pi) \\ -\frac{1}{2}L_{ms} & L_{ms}+L_{ls} & -\frac{1}{2}L_{ms} & L_{ms}\cos(\theta-\frac{2}{3}\pi) & L_{ms}\cos(\theta) & L_{ms}\cos(\theta+\frac{2}{3}\pi) \\ -\frac{1}{2}L_{ms} & -\frac{1}{2}L_{ms} & L_{ms}+L_{ls} & \cos(\theta+\frac{2}{3}\pi) & \cos(\theta-\frac{2}{3}\pi) & \cos(\theta) \\ L_{ms}\cos(\theta) & L_{ms}\cos(\theta-\frac{2}{3}\pi) & L_{ms}\cos(\theta+\frac{2}{3}\pi) & L_{mr}+L_{lr} & -\frac{1}{2}L_{mr} & -\frac{1}{2}L_{mr} \\ L_{ms}\cos(\theta+\frac{2}{3}\pi) & L_{ms}\cos(\theta) & L_{ms}\cos(\theta-\frac{2}{3}\pi) & -\frac{1}{2}L_{mr} & L_{mr}+L_{lr} & -\frac{1}{2}L_{mr} \\ L_{ms}\cos(\theta-\frac{2}{3}\pi) & L_{ms}\cos(\theta+\frac{2}{3}\pi) & L_{ms}\cos(\theta) & -\frac{1}{2}L_{mr} & -\frac{1}{2}L_{mr} & L_{mr}+L_{lr} \end{bmatrix} \begin{bmatrix} i_{sa} \\ i_{sb} \\ i_{sc} \\ i_{ra} \\ i_{rb} \\ i_{rc} \end{bmatrix} \tag{2.3}$$

where

L_{ms} , L_{mr} : Stator and rotor mutual inductances;

L_{ls} , L_{lr} : Stator and rotor leakage inductances;

θ : Rotor angle;

Apply Park transformation into the above equations, the inductor model under d-q coordinate can be expressed in equation (2.4):

$$\left.\begin{aligned} u_{sd} &= R_s i_{sd} + d\varphi_{sd} / dt - \omega_s \varphi_{sd} \\ u_{sq} &= R_s i_{sq} + d\varphi_{sq} / dt + \omega_s \varphi_{sq} \\ u_{rd} &= R_r i_{rd} + d\varphi_{rd} / dt - \omega_s \varphi_{rd} \\ u_{rq} &= R_r i_{rq} + d\varphi_{rq} / dt + \omega_s \varphi_{rq} \end{aligned}\right\} \quad (2.4)$$

where

u_{sd} , u_{sq} , u_{rd} , u_{rq} : Stator and rotor d, q axis voltages;

i_{sd} , i_{sq} , i_{rd} , i_{rq} : Stator and rotor d, q axis currents;

φ_{sd} , φ_{sq} , φ_{rd} , φ_{rq} : Stator and rotor d, q axis flux linkage;

ω_s : Slip angle frequency;

The expressions of the stator and rotor d, q axis flux linkages are shown in equation (2.5),

$$\left.\begin{aligned} \varphi_{sd} &= L_s i_{sd} + L_m i_{rd} \\ \varphi_{sq} &= L_s i_{sq} + L_m i_{rq} \\ \varphi_{rd} &= L_r i_{rd} + L_m i_{sd} \\ \varphi_{rq} &= L_r i_{rq} + L_m i_{sq} \end{aligned}\right\} \quad (2.5)$$

Where L_m is the mutual inductance between the stator and rotor.

After implementing the Park transformation, align the stator flux with the stator d axis flux and let the flux through the q axis be zero (this is the key of space vector control scheme), that is

$$\begin{aligned} \varphi_{sd} &= \varphi_s \\ \varphi_{sq} &= 0 \end{aligned} \quad (2.6)$$

The stator active and reactive power can be expressed as equation (2.7),

$$\left.\begin{aligned} P_s &= -\frac{3}{2} U_s \frac{L_m}{L_{ms}} i_{qr} \\ Q_s &= \frac{3}{2}\left(\frac{U_s^2}{\omega_s L_{ms}} - \frac{U_s L_m i_{dr}}{L_{ms}}\right) \end{aligned}\right\} \qquad (2.7)$$

where

P_s : Stator active power;

Q_s : Stator reactive power;

U_s : Stator voltage;

It can be observed the stator active power depends on the q-axis rotor current and the reactive power depends on the d-axis rotor current. It is convenient to control the active power or reactive power separately by adjusting the d or q axis rotor current and obtain the desired power factor. The stator flux is often required to be aligned with the q axis in order to decouple the power expressions with respect to d and q rotor current. Figure 2.3 shows the block diagram of DFIG control scheme.

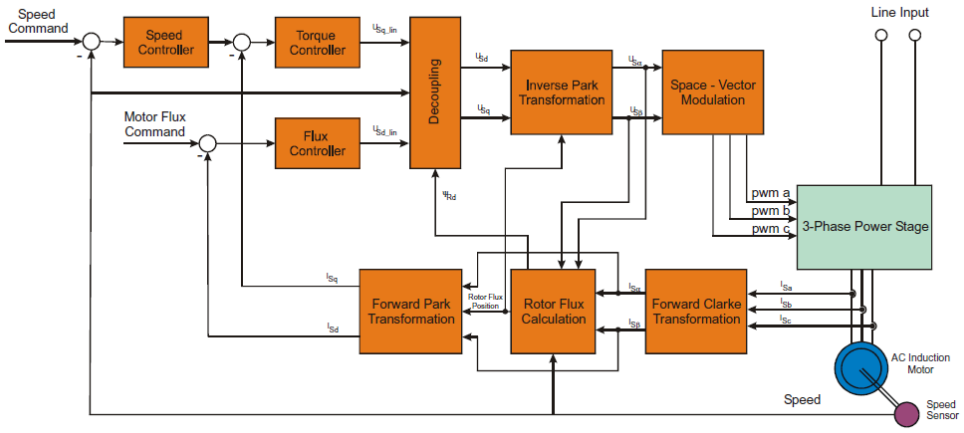

Fig. 2.3 Block diagram of the DFIG vector control [11]

Some of the advantages of the DFIG are that it has reliable speed and better performance than SFIG. However, DFIG is more expensive due to the converter cost and its produced heat and harmonics. Also, the gear box may cause a mechanical problem [12]. In addition, the DFIG has higher maintenance cost.

3) PMSG

In a PMSG shown in figure 2.4, it consists of a wind rotor, a synchronous generator and a back to back converter. The rotor inside the synchronous generator is made by permanent magnet materials and can be designed with a large amount of pairs of poles, so the wind rotor can drive the synchronous generator directly in its rotating speed without increasing the speed by gear box.

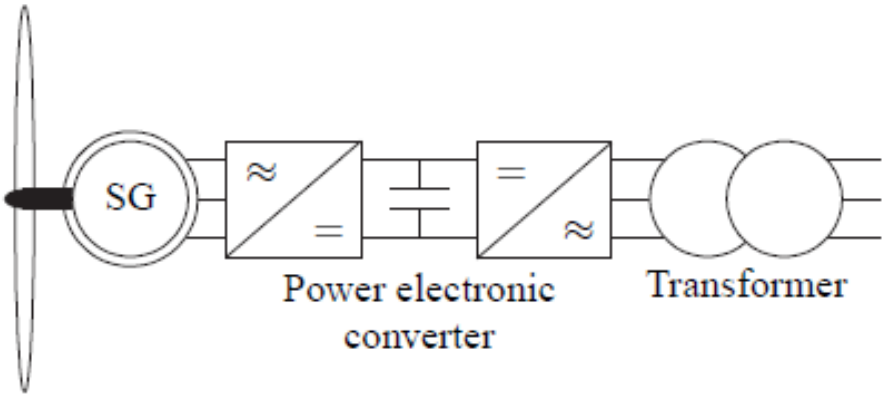

Fig. 2.4 Structure of PMSG

The control scheme of the PMSG converter is the same as DFIG. The difference is that the stator of a PMSG is connected to the main grid through the converter which handles 100% power flow. As a result, the converter produces more wasted heat and claims a higher manufacture requirement. The price of a PMSG converter is much more

expensive than a DFIG. Although the PMSG has larger generation capacity and higher generation efficiency than DFIG, it is still not widely used due to its higher cost.

4) Comparison of the wind generators

Table 2.1 summarizes the features of the three types of wind generators mentioned above.

TABLE 2.1 Comparisons of Different Wind Generators

	Capacity	Gear box	Price	Efficiency
SFIG	Low	Yes	Low	Low
DFIG	Medium	Yes	Medium	Medium
PMSG	High	No	High	High

The above comparison shows that DFIG has acceptable price and efficiency. In addition, it operates at variable speed. Therefore DFIGs are widely used for wind generation.

5) Wind generation forecasting

The generation of wind power depends on the wind speed. According to reference [13], the relationship between the active power generation and wind speed can be expressed by equation (2.8).

$$\left.\begin{array}{l} P_{wt} = 0\ ,\ V_{actual} < V_{cut-in} \\ P_{wt} = aV_{actual}^2 + bV_{actual} + c\ ,\ V_{cut-in} \le V_{actual} < V_{rated} \\ P_{wt} = rated\ power\ ,\ V_{rated} \le V_{actual} \end{array}\right\} \quad (2.8)$$

where

P_{wt} : Wind turbine active generation;

V_{actual} : Actual wind speed;

V_{cut-in} : Cut in wind speed;

V_{rated} : Rated wind speed;

The above variables, parameters *a*, *b*, *c* and *rated power* can be obtained from the manufacture instruction of the wind turbine used.

6) Case study

A case is studied using MATLAB/PowerSystem Simulink. Three separated DFIGs are injected into a 12.47 kv distribution network. The system active load is 3.69 MW and each DFIG has a 1.5 MW generation capacity. The parameters of the DFIG are shown in the following chart.

Nom. Power 1.5MW**;**	**Nom. L-L voltage** 575 v;
Nom. Rotor voltage 1975 v**;**	**Frequency** 60 Hz;
Stator resistance 0.023 p.u. **;**	**Stator inductance** 0.18 p.u.;
Rotor resistance 0.016 p.u. **;**	**Rotor inductance** 0.16 p.u.;
Magnetizing inductance Lm 2.9 p.u;	
Inertia constant H 0.685**;**	**Friction factor F** 0.01 p.u.;
Initial condition slip=-0.2**;**	**Nominal DC bus voltage** 1150 v;
DC bus capacitor 0.000006 F;	**Pairs of poles** 3.

Fig. 2.5 DFIG parameters

The simulation duration is 2.5 seconds. In the initial period of time, the distribution network operates without any DFIGs. Later, at 0.565 second three DFIGs are switched onto the network. Then at 1.2 sec, two unbalaced feeders are connected to the

network. A 3-phase fault occurs at bus #50 at 1.7 sec and the fault clears at 1.7667 sec. The following figures show stator voltage during the simulation and the system diagram.

Stator Voltage

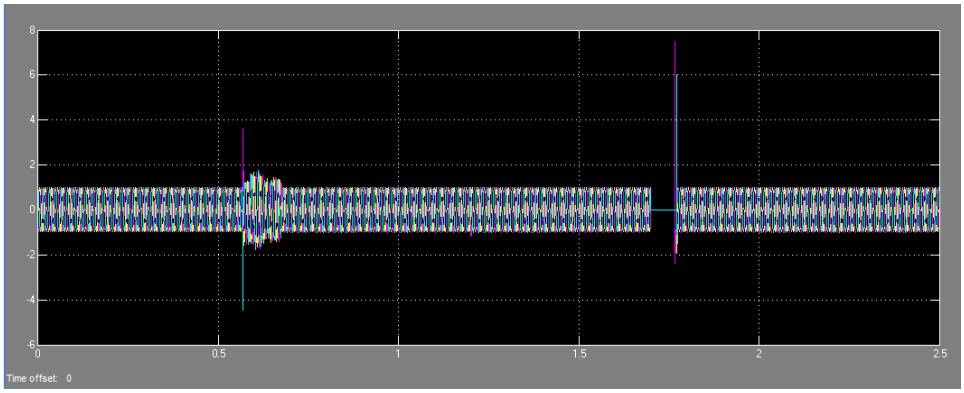

(a) Stator voltage output of the overall simulation;

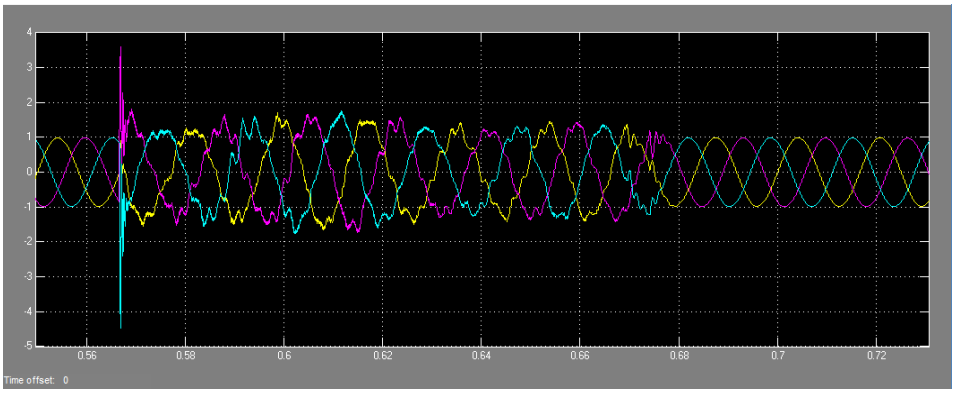

(b) At t=0.565 sec, DFIGs are connected to the network, transient occurs and lasts from 0.565 sec to 0.68 sec;

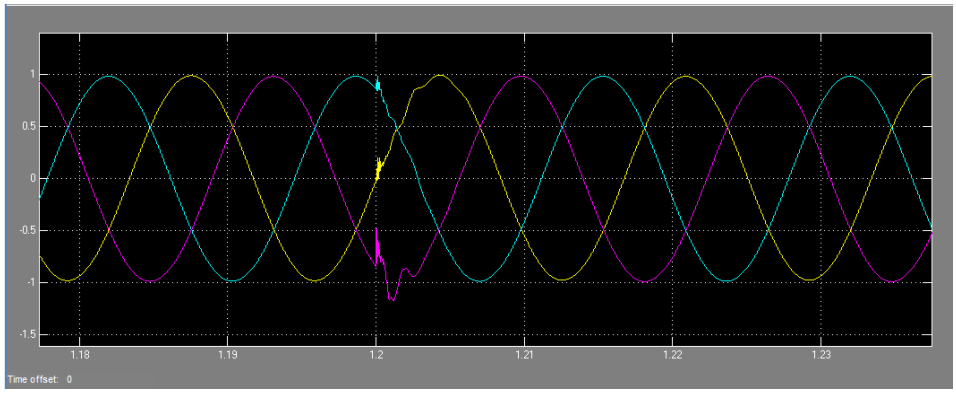

(c) Unbalanced feeders are connected to the grid at t=1.2 sec;

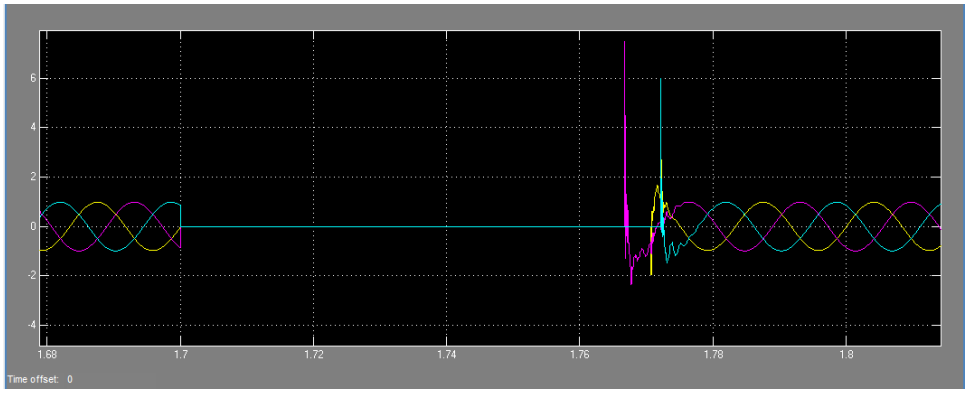

(d) A 3-phase fault occurs at t=1.7 sec at Bus #50 and the fault clears at t=1.7667 sec;

Fig. 2.6 DFIG simulation results

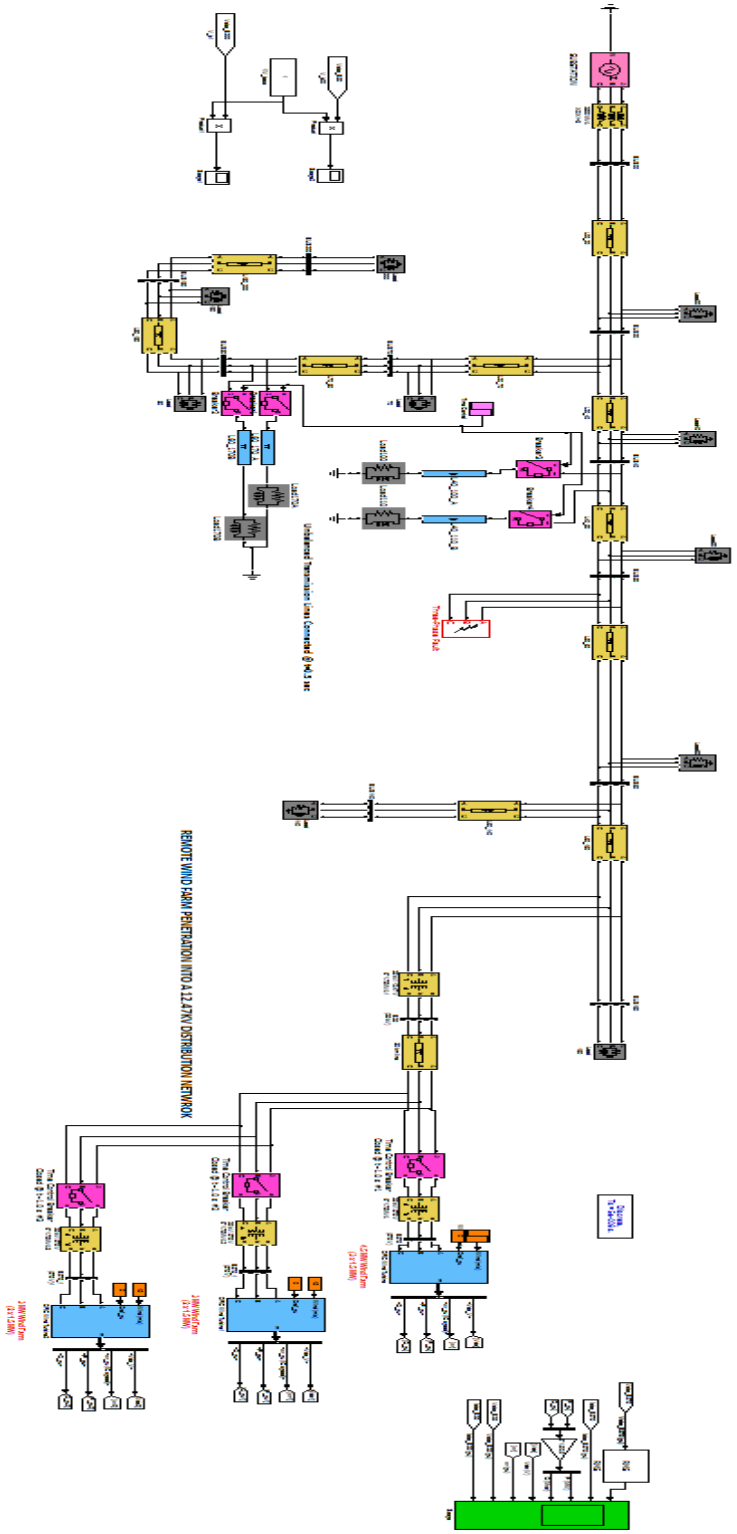

Fig. 2.7 Simulation case using MATLAB

2.2 Photovoltaic Cell

Photovoltaic (PV) is another clean energy source used in power system, which absorbs the solar irradiation and converts it into electric energy. So it is recommended to install PV in an area with good solar irradiation during a year. The average radiation level (ARL, kwh/m^2) can be classified into the following grades in a year:

Perfect sunlight	ARL> 1750 kwh/m^2
Very good sunlight	1400<ARL<1750 kwh/m^2
Good sunlight	1050<ARL<1400 kwh/m^2
Normal sunlight	ARL<1050 kwh/m^2.

According to the composition, PV can be classified into several types, such as silicon type PV including single crystalline Si and multi-crystalline Si, non-silicon type PV, organic type PV, compound type PV and film type PV. Compared with wind turbines, PV occupies less space and has lower cost and zero noise pollution. Moreover, the PV generation fits the load demand very well since the solar irradiation is higher in daytime, as well as the load demand. The utilization of PV in power system is able to reduce the fuel cost and gas emissions. In this research, the silicon type PV is going to be introduced and used in microgrid study. Next sections show the operation principle of silicon type PV.

In the outer sphere of silicon atom, there are four electrons which can be released by absorbing the solar irradiation. When trivalent impurity such as boron and aluminum which is easy to capture electrons is mixed in silicon, it constructs a p-type semiconductor. When pentavalent impurity like phosphorus and arsenic which is easy to

release electrons is mixed in silicon, it constructs an n-type semiconductor. The combination of p and n type semiconductors is called a p-n junction, which is capable of building an internal electric field through the shifting of electrons excited by the solar irradiation. The electrons flow through the external load and a close circuit is constructed. Figure 2.8 shows the operation principle of a PV cell.

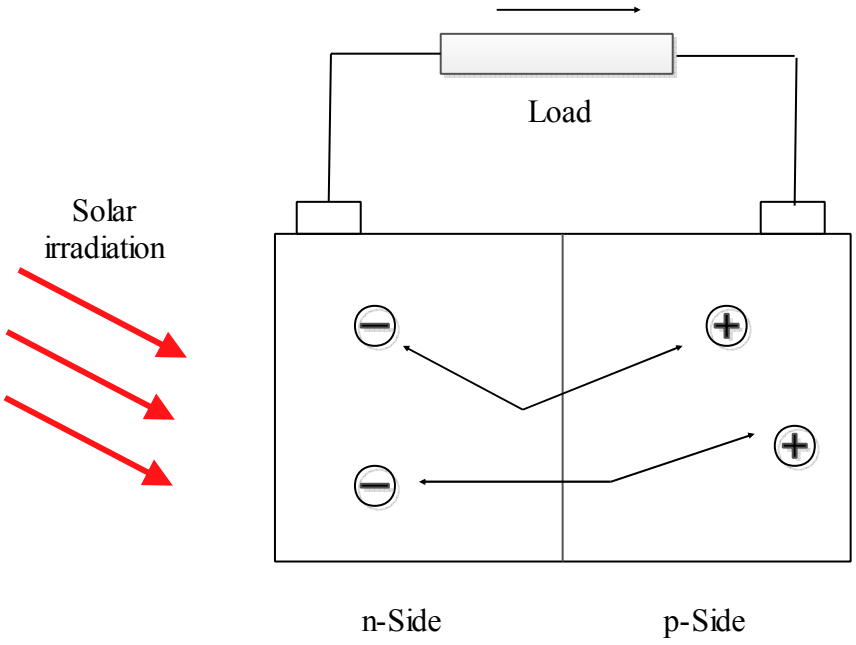

Fig. 2.8 Operation principle of PV cell

The PV V-I curve in figure 2.9 shows the relation between the output current and the external voltage under specific temperatures for solar irradiations. The maximum power point (MPPT) refers to the point with a maximum power output in the curve under specific external voltage and solar irradiation. Normally, a PV cell is controlled by power electronic devices to track the MPPT and get the optimal operation mode. The PV circuit in figure 2.10 can be equivalent to a constant current source in parallel with a diode and a

shunt resistor. The output current *I* equals to the solar generated current I_{ph} subtracted by the current I_D through the diode and the current I_{sh} through the shunt resistor.

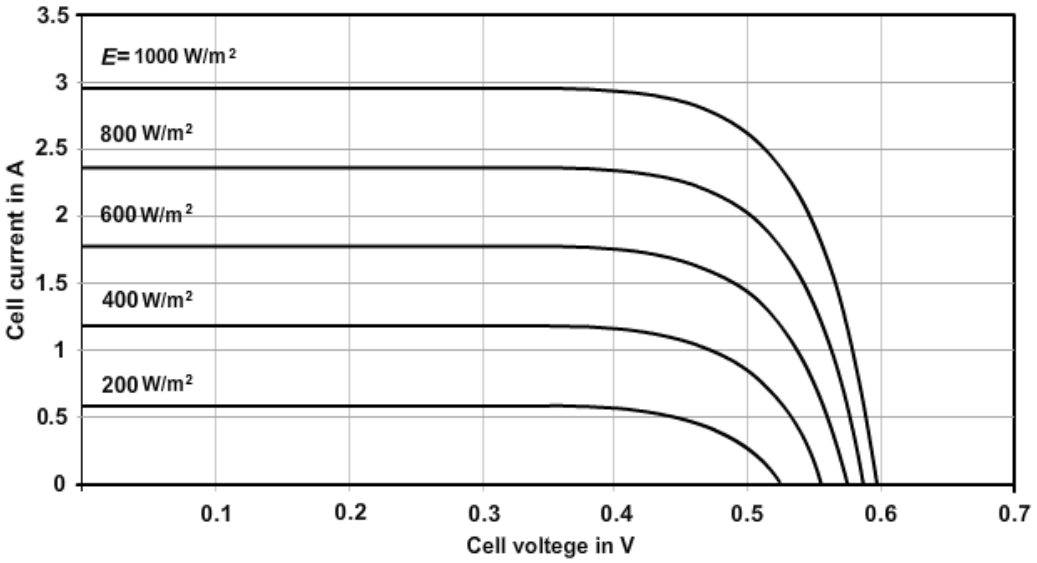

Fig. 2.9 V-I curve of photovoltaic under different solar irradiation [14]

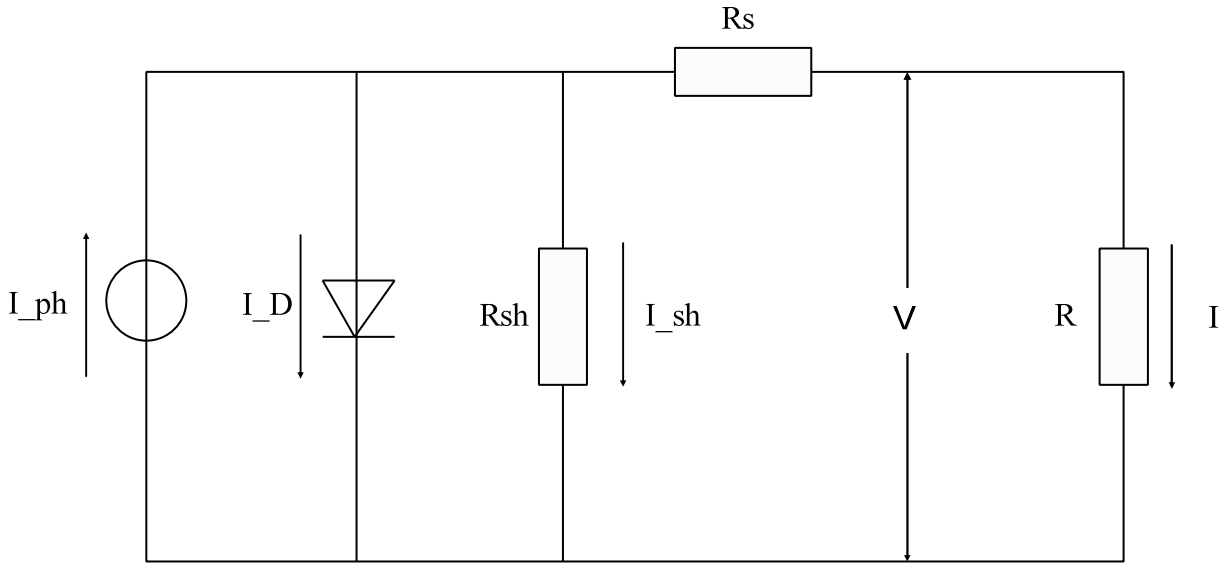

Fig. 2.10 Equivalent circuit of a PV cell [15]

Formulations related to the PV circuit:

$$I = I_{ph} - I_D - I_{sh} \tag{2.9}$$

According to [16], the shunt current can be expressed by equation (2.10):

$$I_D = I_0 \cdot e^{\frac{qV_j}{A_0 kT}} - 1 \tag{2.10}$$

where

I_{ph} : Generated current by absorbing solar energy;

I_D : Current through the diode;

I_{sh} : Current through the shunt resistance;

I_0 : Cell reverse saturation current;

q : Electron charge, equals to 1.6e-19;

V_1 : Open circuit voltage;

A_0 : Curve fitting constant;

k : Boltzmann constant, equals to 1.38e-23;

T : Temperature.

Solar generation forecasting is based on the predicted solar irradiation and temperature. Once the predicted solar irradiation and temperature are estimated, the solar generation can be obtained according to the manufacture instructions.

2.3 Microturbine

Microturbine is a term for gas turbine which has a small size and high speed. A microturbine normally contains a gas turbine, a recuperator (heat exchanges) to obtain high energy utilization efficiency, a gas compressor to provide natural gas with a desired pressure, a control system regulating the output current and the basic electrical system. The detailed knowledge of microturbines can be reached in [17-19].

The operation principle of a microturbine includes the following steps:

Step 1: Fresh air blows into the compressor, and the compressor increases the pressure of the fresh air.

Step 2: The high-pressure air is mixed with the fuel and burnt at a constant pressure in the combustor.

Step 3: The burnt gas with high flowing speed enters the turbine and drives the turbine to rotate.

Step 4: The magnetic field within the rotor reacts with the stator and produces electric energy.

Step 5: The produced current is regulated by the converter to obtain good quality current with synchronous frequency.

According to [18], the cost function of microturbine is expressed as

$$C_{MT} = C_{ng} \sum_{j} \frac{P_j}{\eta_j} \tag{2.11}$$

where

C_{MT} : Cost of the microturbine generation;

C_{ng} : The natural gas price to supply the microturbine;

P_j : The power output during time interval *j*;

η_J : The microturbine efficiency at interval *j*.

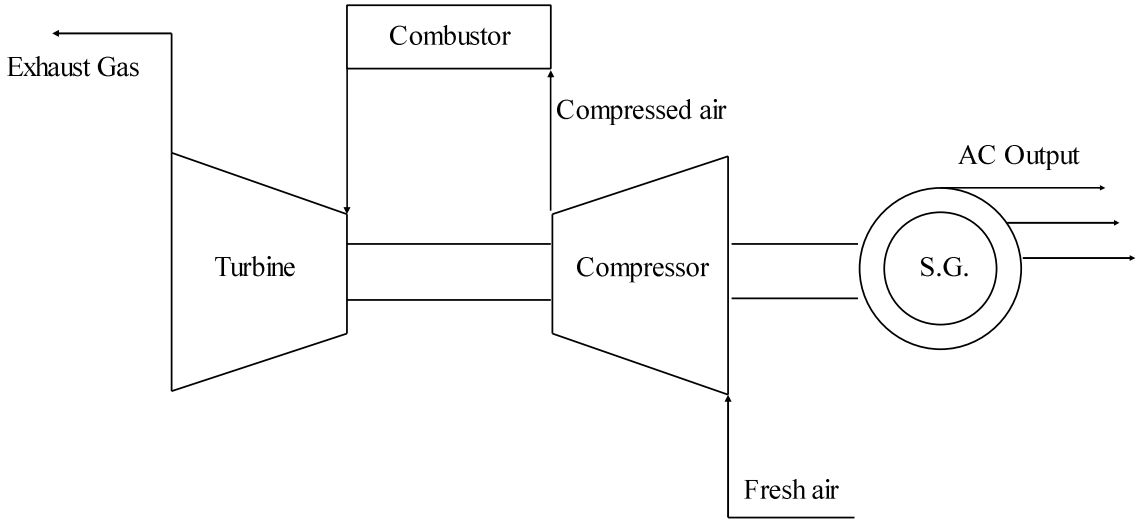

Fig. 2.11 Structure of a microturbine

2.4 Fuel Cell

Fuel cell is one type of distributed energy resources converting the chemical energy into electrical energy through an oxidation reaction. The fuel cell technology was firstly proposed by the Welsh physicist William Grove in 1839 and the first commercial application of fuel cell was carried out by NASA space generating power for probes, satellites and space capsules [20-21]. Generally, a fuel cell consists of an anode as the positive side, a cathode as the negative side and electrolyte allowing the ions pass through. The anode is usually made up of very fine platinum powder. The cathode is

often made by nickel. The electrolyte substance defines the type of fuel cell, and hydrogen is commonly used as the oxidizing fuel in the chemical reaction. Figure 2.12 depicts the fuel cell operation principle.

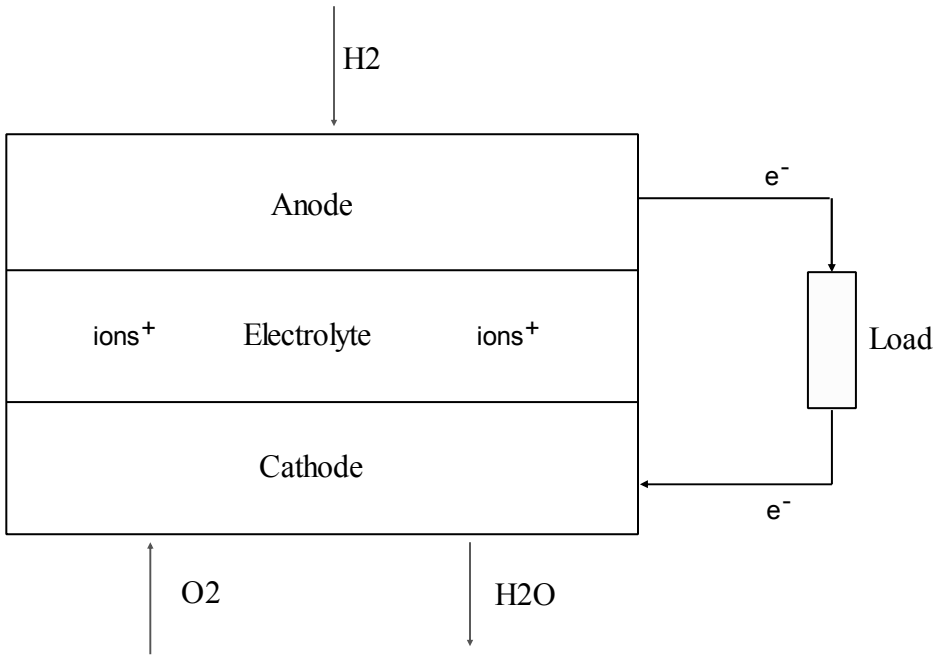

Fig. 2.12 Structure of a fuel cell

At the anode, the hydrogen is supplied and oxidized, producing electrons and ions moving towards to the external load. At the cathode, the ions react with the cathode substances and are turned into wastes like water and heat.

Anode reaction:

$$2H_2 + 2O_2^{-2} \rightarrow 2H_2O + 4e^-$$

Cathode reaction:

$$O_2 + 4e^- \rightarrow 2O_2^{-2}$$

Overall cell reaction:

$$2H_2 + O_2 \rightarrow 2H_2O$$

The efficiency of a fuel cell is about 40% - 60%, and may be up to 80% if the waste heat is used. Based on reference [22], the cost function of fuel is shown in equation (2.12),

$$C_{FC} = C_{fuel} \sum_j \frac{P_j}{\eta_j} \tag{2.12}$$

where

C_{FC} : The cost of fuel cell generation;

C_{fuel} : The fuel cost;

P_j : The power output during time interval *j*;

η_J : The fuel cell efficiency at interval *j*.

2.5 Energy Storage System

Energy storage system (ESS) in power system is a device storing energy when the system has surplus energy and delivering energy during peak load periods. ESS is usually coordinated with a wind farm or a group of PV cells and stores the excess energy. There are various types of ESS with different ranges of storing capacity, such as super capacitor, battery, flywheel and so on. The super capacitor is an electric double-layer capacitor and based on carbon technology. Super capacitor has the highest capacity density and fast charging or discharging speed. It can work within a larger range of temperature from -40 ℃ to +70 ℃. The service life of super capacitor is longer than other storage devices [23]. The flywheel utilizes the electric machine and stores the electric energy by transforming it into mechanical energy. It has high efficiency, long service life, zero environment pollution and fast charging or discharging speed [24]. The battery stores and generates the electric energy by electrochemical reactions [25]. Battery usually has a low cost and is easy to install. Normally, the super capacitor and flywheel have larger storing capacities than battery and the prices are expensive, so battery is recommended to be used as small size storage in microgrid.

There are many types of battery, such as lead-acid battery, Ni/Cd, Zn/Br, Na/S and so on. In this research, the lead-acid battery is selected and modeled. A lead-acid battery consists of a positive electrode made by lead dioxide, a negative electrode made by porous lead and electrolyte made by sulfuric acid containing aqueous ions (H^+ and SO_4^{-2}). The lead-acid battery construction and chemical reactions on both electrodes are shown in Figures 2.13-2.15.

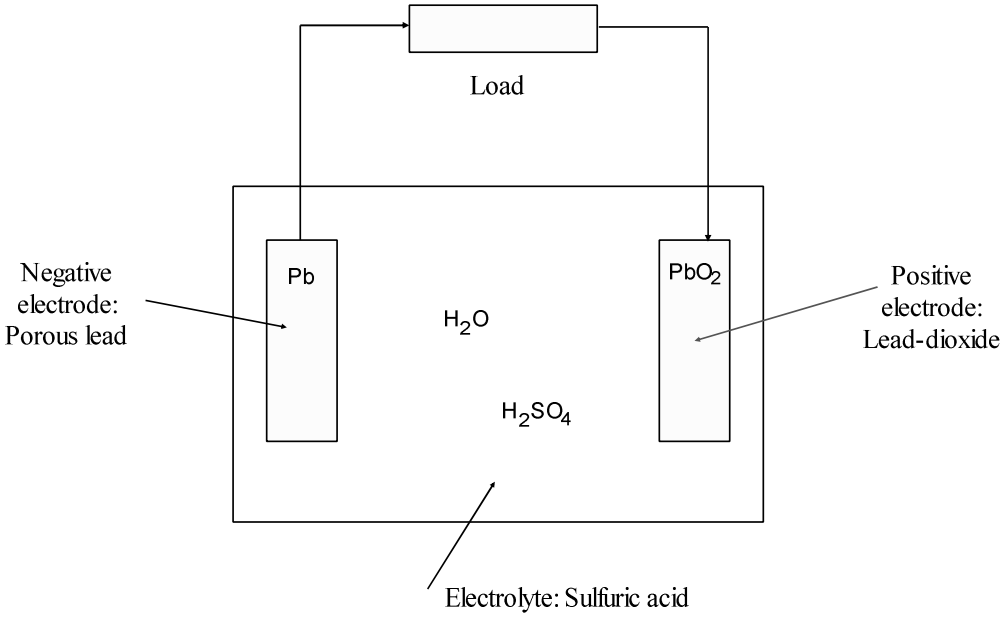

Fig. 2.13 Construction of a lead-acid battery

On the negative electrode, the charged sulfate ion moves towards the lead atom and reacts with it. For each lead atom, two electrons are released after each reaction.

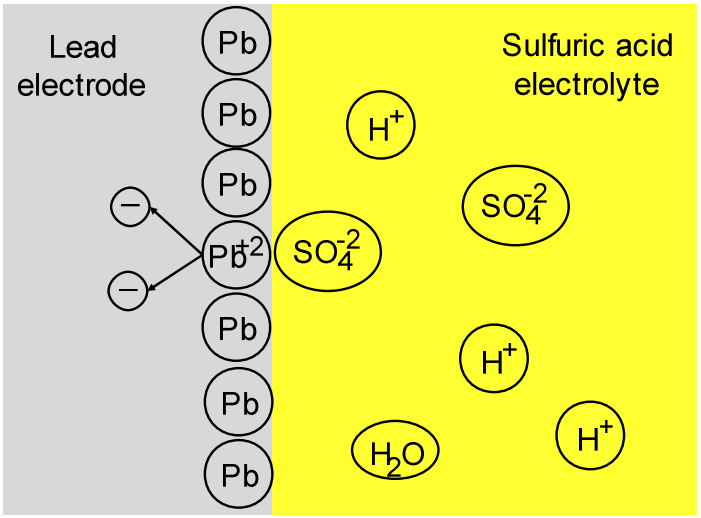

$$Pb + SO_4^{-2} \rightarrow PbSO_4 + 2e^-$$

Fig. 2.14 Chemical reaction on negative electrode

On the positive electrode, the charged sulfate and hydrogen ions approach lead-dioxide, as well the lead-dioxide receives the electrons from the negative electrode, and the reaction on the positive side produces lead sulfate and water.

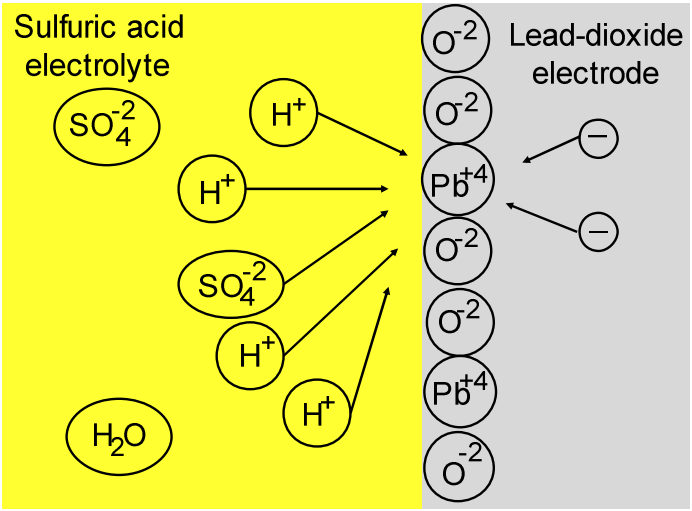

$$PbO_2 + SO_4^{-2} + 2e^- \rightarrow PbSO_4 + 2H_2O$$

Fig. 2.15 Chemical reaction on positive electrode

During the discharging process, the external load allows the electrons to flow from negative side to the positive side. This process reduces the voltages at the electrodes and weakens the acid electrolyte. While in the charging process, the external voltage is added to the battery and let the electrons move from the positive side to negative side. The charging process increases the voltage between the electrodes and the acid electrolyte becomes stronger. The equivalent circuit of a lead-acid battery can be shown in Figure 2.16.

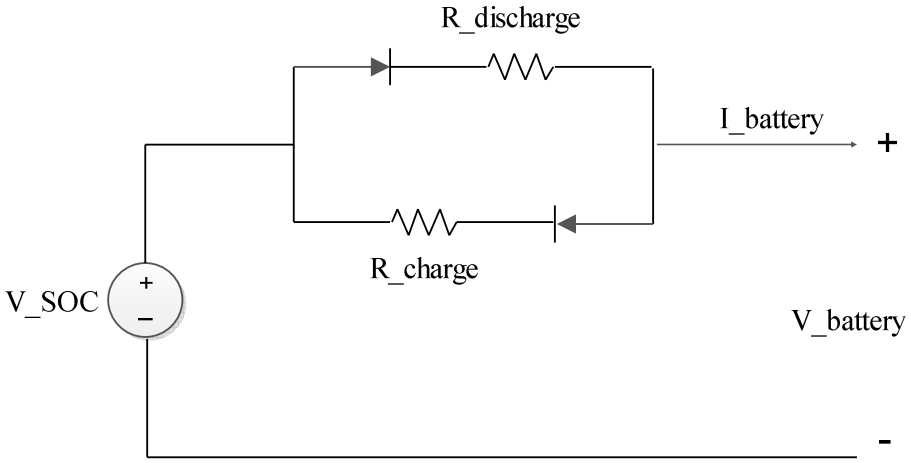

Fig. 2.16 Lead-acid battery equivalent circuit

SOC stands for state of charge and is a percentage value. To avoid over-use or over charge, the SOC of a battery is set between 20% and 100%. The relationship between the battery resistance and the SOC can be shown in Figure 2.8 [26]. It can be seen, when the battery is in charging state, the resistance increases as SOC increases; when it is in discharging sate, the resistance decreases as SOC increases.

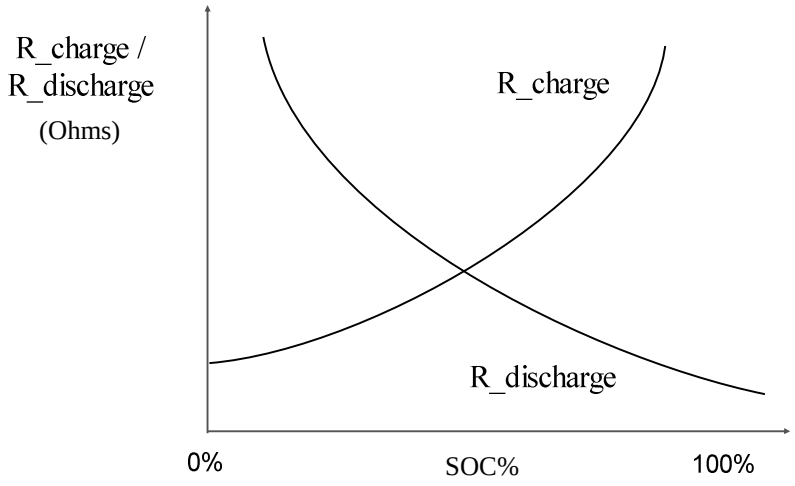

Fig. 2.17 Relation between the SOC and the battery resistance

The charging energy efficiency of a lead-acid battery is affected when reactions other than reversal of sulfate occur. The variation of SOC depends on the charging or discharging power, the charging efficiency and battery storing capacity. The SOC at time t+1 equals to the SOC at time t subtracting the SOC variation during this interval. Hence, the SOCs of each two adjacent time intervals are related.

$$soc(t+1) = soc(t) - \frac{\eta_t P_{ess}(t)}{W_{ess}}$$

$$soc^{\min} \le soc(t+1) \le soc^{\max} \tag{2.13}$$

where

η_t : Charging or discharging efficiency;

W_{ess} : Battery storing capacity;

$P_{ess}(t)$: Battery output power at time *t*.

CHAPTER THREE

OPTIMIZATION MODEL FOR ENERGY MANAGEMENT IN MICROGRIDS

In this chapter, the model for energy management in microgrid is built, then the formulations of the model are re-arranged in preparation for the proposed algorithm. In the third section, the advanced dynamic programming (ADP) algorithm is introduced and used to solve the model. Finally, a microgrid benchmark is tested by the proposed algorithm and simulation results are shown and analyzed.

3.1 Model Formulations

According to reference [27], some prerequisite information for a 24-hours energy management should be known in advance. The information is as follows:

- Hourly load forecasting for the next day;
- Hourly wind and PV generation forecasting;
- DERs' cost functions, parameters and power limits;
- Initial charge condition of ESS.

Of course, the time interval can also be set to 15 min or other time interval rather than one hour.

In this model, two possible operation policies are defined and included [28]. In policy I, a microgrid is disconnected from the main grid and operates in a stand-alone mode. While in Policy II, a microgrid is penetrated to the main grid and has power exchange with the main grid. In this case, it can either send (sell) power to the main grid or receive (buy) power from the main grid.

a) Market Policy I

In policy I, the load demands in a microgrid is satisfied by its local generation. General formulations are as follows.

Objective function:

$$Min \quad \sum_{t=1}^{n}\sum_{j=1}^{m} F_j(P_j(t)) \cdot \tau_j(t) + s_j(t) \tag{3.1}$$

where,

$\tau_j(t) = 1$ if the j^{th} unit is on at time t;

$\tau_j(t) = 1$ if it is off.

The cost functions are:

$$F_j(P_j(t)) = b_j P_j(t) + c_j \text{ (Micro-turbine or fuel cell),}$$

$$F_j(P_j(t)) = a_j P_j(t)^2 + b_j P_j(t) + c_j \text{ (Diesel engine),}$$

Here a_j, b_j and c_j are corresponded parameters for each cost function; the startup cost function is

$$s_j(t) = \begin{cases} sc_j, & if \quad \tau_j(t) - \tau_j(t-1) = 1 \\ 0, & otherwise \end{cases},$$

noting that sc_j is the startup cost of unit j.

The objective function is subjected to the following constraints:

1) Power output of the j^{th} unit at time t

$$P_j^{\min} \le P_j(t) \le P_j^{\max}$$

2) Supply balance equality of the generations and loads

$$\sum_{j=1}^{m} P_j(t) = P_{load}(t) - P_{wind}(t) - P_{pv}(t) - P_{ess}(t) \tag{3.2}$$

3) ESS power output

$$P_{ess}^{\min} \le P_{ess}(t) \le P_{ess}^{\max}$$

$P_{ess}(t) > 0$, ESS is discharging power;

$P_{ess}(t) < 0$, ESS is charging power;

$P_{ess}(t) = 0$, ESS has zero generation.

4) Dynamic performance of ESS

$$soc(t+1) = soc(t) - \frac{\eta_t P_{ess}(t)}{W_{ess}}$$

$$soc^{\min} \le soc(t+1) \le soc^{\max} \tag{3.3}$$

Where n is the total time intervals for a scheduling day; m indicates the number of all types of dispatchable units; soc stands for state of charge; η_t is the ESS charging or discharging efficiency; W_{ess} denotes the ESS capacity; $P_{load}(t)$, $P_{wind}(t)$ and $P_{pv}(t)$ separately represent the forecasted loads, wind generation and photovoltaic generation at time t.

b) Market Policy II

Models in policy II are similar to policy I except the objective function and the balance equality.

Case I: Buying power from main grid

The objective function is

$$Min \sum_{t=1}^{n}\{c_{grid}(t)P_{grid}(t)+\sum_{j=1}^{m}F_j(P_j(t))\cdot\tau_j(t)+s_j(t)\} \quad (3.4)$$

where $c_{grid}(t)$ is the electricity price in main grid at time *t*; $P_{grid}(t)$ is the received power from the main grid, $P_{grid}(t)>0$.

The balance equation in this case is

$$\sum_{j=1}^{m}P_j(t)=P_{load}(t)-P_{wind}(t)-P_{pv}(t)-P_{ess}(t)-P_{grid}(t). \quad (3.5)$$

Case II: Selling power to main grid

The objective function becomes

$$Max \sum_{t=1}^{n}\{-c_{grid}(t)P_{grid}(t)-\sum_{j=1}^{m}F_j(P_j(t))\cdot\tau_j(t)+s_j(t)\} \quad (3.6)$$

where $c_{grid}(t)$ is the electricity price in main grid at time *t*; $P_{grid}(t)$ is the power sent to main grid, $P_{grid}(t)<0$.

The balance equation in this case is

$$\sum_{j=1}^{m}P_j(t)=P_{load}(t)-P_{wind}(t)-P_{pv}(t)-P_{ess}(t)-P_{grid}(t). \quad (3.7)$$

Above all, during the periods receiving power from main grid, a microgrid is supposed to minimize the production cost and the expense purchasing power from the main grid; when the microgrid sells power to the main grid, the optimal goal is to maximize the profit which is the revenue minus the fuel cost consumption.

3.2 Formulation Arrangement

In order to apply the proposed optimization technique to this research, the formulations in both policy I and II are required to be transformed into a more suitable form.

Let x_i be a state vector including the power output of dispatchable units at time *i*; let u_i be a decision vector consisting of the planning generation adjustment for each dispatchable unit; function g_i reflects the relation between adjacent states; function Γ_i is the cost function at time *i*. To minimize the total cost, the recommended formulations are shown in equation (3.8):

$$\min \quad \Gamma = \sum_{i}^{N-1} \Gamma_i(x_i, u_i) + \Gamma_N(x_N), \tag{3.8}$$

which is subjected to the following constraints

$$\left.\begin{array}{l} x_{i+1} = g_i(x_i, u_i) \\ c_{iE}(x_i, u_i) = 0, \qquad c_{NE}(x_N) = 0 \\ c_{iI}(x_i, u_i) \le 0, \qquad c_{NI}(x_N) \le 0, \end{array}\right\} \tag{3.9}$$

where i=1, 2, …, *N-1*.

In this discrete-time system, it is expected to find the optimal control variables $u_1, u_2, .., u_{N-1}$ and the initial state variable x_1 which aim to minimize the goal function. The functions g_i, Γ_i, c_{iE}, and c_{iI} are all twice differentiable.

For policy I, the following transformation of formulations are:

$$x_i = \left[P_1(i) \quad P_2(i) \quad ... \quad P_m(i) \quad P_{ess}(i) \quad soc(i) \right]^T$$

$$u_i = \begin{bmatrix} \Delta P_1(i) & \Delta P_2(i) & .. & \Delta P_m(i) & \Delta P_{ess}(i) \end{bmatrix}^T$$

$$\Gamma_i(x_i, u_i) = x_i^T y_i + x_i^T Q_i x_i + v_i$$

$$\Gamma_N(x_i) = x_N^T y_N + x_N^T Q_N x_N + v_N$$

$$g_i(x_i, u_i) = \begin{bmatrix} 1 & 0 & 0 & 0 & 0 & 0 \\ 0 & 1 & 0 & 0 & 0 & 0 \\ .. & .. & .. & .. & .. & .. \\ 0 & 0 & 0 & 1 & 0 & 0 \\ 0 & 0 & 0 & 0 & 1 & 0 \\ 0 & 0 & 0 & 0 & 0 & 0 \end{bmatrix} x_i + \begin{bmatrix} 1 & 0 & 0 & 0 & 0 \\ 0 & 1 & 0 & 0 & 0 \\ 0 & 0 & .. & 0 & 0 \\ 0 & 0 & 0 & .. & 0 \\ 0 & 0 & 0 & 0 & 1 \\ 0 & 0 & 0 & 0 & 0 \end{bmatrix} u_i$$

$$c_{iE}(x_i, u_i) = \begin{bmatrix} 1 & 1 & .. & .. & 1 & 0 \end{bmatrix} x_i + [-P_{load}(i) + P_{wind}(i) + P_{pv}(i)]$$

$$c_{iI}(x_i, u_i) = \begin{bmatrix} 1 & 0 & 0 & 0 & 0 & 0 & 0 & 0 \\ -1 & 0 & 0 & 0 & 0 & 0 & 0 & 0 \\ 0 & 1 & 0 & 0 & 0 & 0 & 0 & 0 \\ .. & .. & .. & .. & .. & .. & .. & .. \\ 0 & 0 & 0 & 0 & 0 & 0 & 1 & 0 \\ 0 & 0 & 0 & 0 & 0 & 0 & -1 & 0 \\ 0 & 0 & 0 & 0 & 0 & 0 & \frac{-\eta_i}{W_{ess}} & 1 \\ 0 & 0 & 0 & 0 & 0 & 0 & \frac{\eta_i}{W_{ess}} & 1 \end{bmatrix} x_i + \begin{bmatrix} -P_1^{\max} \\ P_1^{\min} \\ -P_2^{\max} \\ .. \\ -P_{ess}^{\max} \\ P_{ess}^{\min} \\ -soc^{\max} \\ soc^{\min} \end{bmatrix}$$

$$c_{NI}(x_N) = \begin{bmatrix} 1 & 0 & 0 & 0 & 0 & 0 & 0 & 0 \\ -1 & 0 & 0 & 0 & 0 & 0 & 0 & 0 \\ 0 & 1 & 0 & 0 & 0 & 0 & 0 & 0 \\ .. & .. & .. & .. & .. & .. & .. & .. \\ 0 & 0 & 0 & 0 & 0 & 0 & 1 & 0 \\ 0 & 0 & 0 & 0 & 0 & 0 & -1 & 0 \\ 0 & 0 & 0 & 0 & 0 & 0 & \frac{-\eta_N}{W_{ess}} & 1 \\ 0 & 0 & 0 & 0 & 0 & 0 & \frac{\eta_N}{W_{ess}} & 1 \end{bmatrix} x_i + \begin{bmatrix} -P_1^{\max} \\ P_1^{\min} \\ -P_2^{\max} \\ .. \\ -P_{ess}^{\max} \\ P_{ess}^{\min} \\ -soc^{\max} \\ soc^{\min} \end{bmatrix}.$$

The dimension of state vector is m+2, while the dimension of the decision vector is m+1. In the cost function Γ_i, the vector y_i, matrix Q_i and constant v_i are related to the cost functions of the DERs used in microgrid.

For policy II, one additional variable is needed for both state vector and decision vector. The added element represents the power exchange with the main grid. The state vector and decision vector for policy II are shown in (3.10).

$$\left.\begin{aligned} x_i &= \begin{bmatrix} P_1(i) & P_2(i) & .. & P_m(i) & P_{ess}(i) & P_{grid}(i) & soc(i) \end{bmatrix}^T \\ u_i &= \begin{bmatrix} \Delta P_1(i) & \Delta P_2(i) & .. & \Delta P_m(i) & \Delta P_{ess}(i) & \Delta P_{grid}(i) \end{bmatrix}^T \end{aligned}\right\} \quad (3.10)$$

The minimum and maximum limits of the grid power exchange could be set as a large amount or the capacity of the transformer linking the main grid and the microgrid.

3.3 Optimization Technique

First of all, it is necessary to give a brief introduction of Multi-Stage Decision Process (MSDP). MSDP represents a dynamic behavior of successive stages in a discrete time system and finds an optimal path of all stages in order to maximize the benefit or minimize the cost in overall stages. Dynamic programming is a sophisticated approach for studying MSDP. However, an MSDP problem can be much more complex with hard constraints, uncertainties and multi-parameters. Methods in resolving such complicated MSDP problems were presented in [8]-[9], [29]-[30].

In an MSDP problem, for a specific stage, it contains several system states determining the current stage's cost. Then, a set of decision variables acts on the current

states and generates new system states for the next stage. This procedure repeats till the last stage. The overall purpose is to find a best path of states transitions leading to a minimal summation of costs of all stages. A chain of stages is shown in Fig. 3.1.

MSDP can be formulated with equations (3.11),

$$\left.\begin{aligned} & x^{k+1} = f^k(x^k, u^k),\ x^k \in X,\ u^k \in U^k,\ k \in \{0,1,\ldots,N-1\} \\ & V^N(x^N) = \min_{u^0,\ldots,u^N}\left[g^N(x^N) + \sum_{k=0}^{N-1} g^k(x^k, u^k) \right], \end{aligned}\right\} \tag{3.11}$$

where

k : The number of time intervals;

x^k : The state vector at stage k;

u^k : The decision vector at stage k;

f^k : The state transition functions;

g^k : The cost function of the state and decision variables at stage k;

V^N : The summation of costs of all *N* stages.

At stage *k*, the objective function and constraints are shown below,

$$V^k(x^k) = \min_{u^k \in U^k}\left[g^k(x^k, u^k) + V^{k-1}(x^{k-1}) \right] \tag{3.12}$$

Subjected to $u_{\min}^{k-1} \le u^{k-1} \le u_{\max}^{k-1}$

$$x_{\min}^k \le x^k \le x_{\max}^k$$

$$x^k = f^{k-1}(x^{k-1}, u^{k-1}),$$

where $u_{\min}^{k-1}$, $u_{\max}^{k-1}$ are limits for decision variables, $x_{\min}^k$, $x_{\max}^k$ are limits for state

variables, V^k denotes the total cost when at stage k.

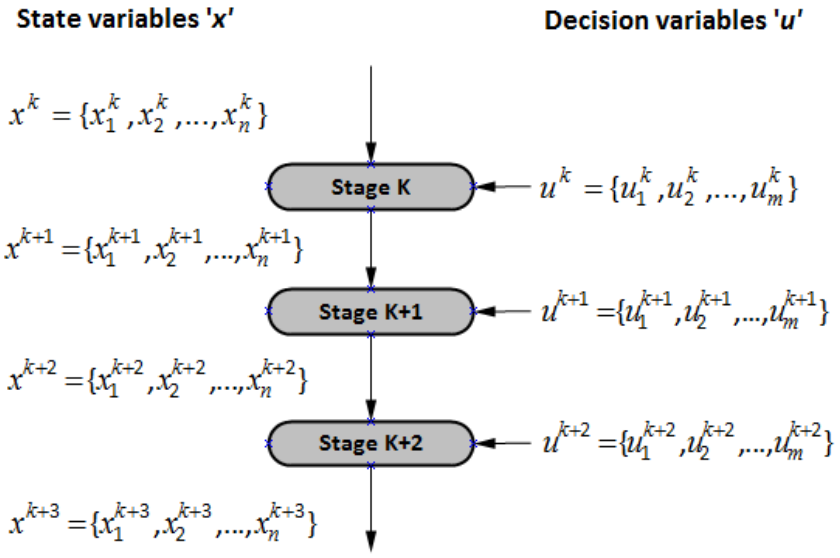

Fig. 3.1 Multi-stage decision process

The optimal energy management model built above is actually a multi-parametric quadratic programming constrained by dynamic programming, which belongs to the class of MSDP problems. In reference [9], the authors proposed a powerful technique to solve the MSDP problem by combing the sequential quadratic programming (SQP), the interior-point method and the conventional dynamic programming together. This method is also called Advanced Dynamic Programming (ADP). The ADP method is proved to have a great performance for discrete-time optimal control constrained by dynamic programming, and widely applied into real guidance problems. In this research, the ADP method is selected as the tool solving the proposed model. In the following parts, at first the SQP and the interior-point methods will be implemented on the model, and then the

modified dynamic programming method proposed in [9] is used to solve the model and obtain the optimal solutions.

1) SQP method

According to the formulations in section 3.2, the equivalent formulations can be expressed as follows using SQP method:

Min

$$\Gamma_q = \sum_{i}^{N-1}[v_i + x_i^T y_i + u_i^T z_i + (x_i^T Q_i x_i + 2x_x^T R_i u_i + u_i^T S_i u_i)/2] + \Gamma_N + x_N^T y_N + x_N^T Q_N x_N /2 \tag{3.13}$$

subjected to

$$x_{i+1} = A_i x_i + B_i u_i$$

$$A_{iE} x_i + B_{iE} u_i + \hat{c}_{iE} = 0, \quad A_{NE} x_N + \hat{c}_{NE} = 0,$$

$$A_{iI} x_i + B_{iI} u_i + \hat{c}_{iI} \le 0, \quad A_{NI} x_N + \hat{c}_{NI} \le 0.$$

The purpose of SQP method is to leave the model with only linear and quadratic terms.

2) Equivalent formulations using interior-point method

According to the above SQP formulations, by applying Lagrangian multipliers and adding slack variables into the inequalities in constraints, a new formulation is shown below. At iteration *k*, it aims to minimize

$$\begin{aligned} L_q^k = \sum_{i}^{N-1}[v_i + \tilde{x}_i^T y_i + \tilde{u}_i^T z_i + (\tilde{x}_i^T Q_i \tilde{x}_i + 2\tilde{x}_i^T R_i \tilde{u}_i + \tilde{u}_i^T S_i \tilde{u}_i)/2] \\ + (\bar{A}_{iE} \tilde{x}_i + \bar{B}_{iE} \tilde{u}_i + \bar{c}_{iE})^T \tilde{\lambda}_{iE} + (\bar{A}_{iI} \tilde{x}_i + \bar{B}_{iI} \tilde{u}_i + \bar{c}_{iI})^T \tilde{\lambda}_{iI} - \tilde{\lambda}_{iI}^T \bar{G}_i \tilde{\lambda}_{iI}/2] \\ + \tilde{x}_N^T \bar{y}_N + \tilde{x}_N^T Q_N \tilde{x}_N + (\bar{A}_{NE} \tilde{x}_N + \bar{c}_{NE})^T \tilde{\lambda}_{NE} + (\bar{A}_{NI} \tilde{x}_N + \bar{c}_{NI})^T \tilde{\lambda}_{NI} - \tilde{\lambda}_{NI}^T \bar{G}_N \tilde{\lambda}_{NI}/2 \end{aligned} \tag{3.14}$$

It is defined that

$$\tilde{z}=\begin{bmatrix}\tilde{u}_1\\ ..\\ \tilde{u}_{N-1}\\ \tilde{x}_1\end{bmatrix},\ \tilde{\zeta}=\begin{bmatrix}\tilde{\lambda}_{1E}\\ ..\\ \tilde{\lambda}_{NE}\end{bmatrix},\tilde{\lambda}=\begin{bmatrix}\tilde{\lambda}_{1I}\\ ..\\ \tilde{\lambda}_{NI}\end{bmatrix},\tilde{s}=\begin{bmatrix}\tilde{s}_{1I}\\ ..\\ \tilde{s}_{NI}\end{bmatrix}. \tag{3.15}$$

The approach in solving $(\tilde{z},\tilde{\zeta},\tilde{\lambda},\tilde{s})$ in each iteration is given in the appendix B.

3) Total algorithm procedures

Given $\delta>0$, $k=0$ and $(z^0,\xi^0,\lambda^0,s^0)$, where $\lambda^0>0$ and $\xi^0>0$. The residual terms are defined as:

$$\left.\begin{aligned}
(r_1^k)^2 &= \sum_{i=1}^{N-1}(\partial L_q^k/\partial\tilde{u}_i)^T(\partial L_q^k/\partial\tilde{u}_i),\\
(r_2^k)^2 &= \sum_{i=1}^{N}(A_{iE}x_i^k+B_{iE}u_i^k+\hat{c}_{iE})^T(A_{iE}x_i^k+B_{iE}u_i^k+\hat{c}_{iE})\\
(r_3^k)^2 &= \sum_{i=1}^{N}(A_{iI}x_i^k+B_{iI}u_i^k+\hat{c}_{iI}+s_{iI}^k)^T(A_{iI}x_i^k+B_{iI}u_i^k+\hat{c}_{iI}+s_{iI}^k)\\
(r_4^k)^2 &= \sum_{i=1}^{N}[\min(\lambda_{iI}^k,s_{iI}^k)]^T[\min(\lambda_{iI}^k,s_{iI}^k)].
\end{aligned}\right\} \tag{3.16}$$

As the solution set approaches on optimum point, the summation of all residual terms should approach zero.

The following steps are carried out to achieve the optimal solutions.

Step 1:

Calculate the residual value r^k

$$r^k=\sqrt{(r_1^k)^2+(r_2^k)^2+(r_3^k)^2+(r_4^k)^2},$$

If $r^k<\delta$, then proceed to step 5.

Step 2:

Let

$d_k = -diag(\lambda^k)diag(s^k)e$,

$c_{iI}^k = A_{iI}x_i^k + B_{iI}u_i^k + \hat{c}_{iI}$,

where $e = \begin{bmatrix} 1 & 1 & .. & 1 \end{bmatrix}^T$.

The affine scaling predictor direction $(\tilde{z}_a, \tilde{\zeta}_a, \tilde{\lambda}_a, \tilde{s}_a)$ is solved by using the method introduced in appendix B.

Then, calculate:

$\mu_k = (\lambda^k)^T \frac{s^k}{n_2}$, where n_2 is the dimension of s^k;

$\alpha_a = \arg\ \max\{\alpha \in [0,1] \mid \lambda^k + \alpha\tilde{\lambda}_a \geq 0, s^k + \alpha\tilde{s}_a \geq 0\}$;

$\mu_a = (\lambda^k + \alpha\tilde{\lambda}_a)^T \frac{1}{n_2}(s^k + \alpha_a\tilde{s}_a)$

the centering parameter is defined as $\sigma = (\frac{\mu_a}{\mu_k})^3$.

Step 3:

Let $d_k = -diag(\lambda^k)diag(s^k)e - diag(\tilde{\lambda}_a)diag(\tilde{s}_a)e + \sigma\mu_k e$

$c_{iI}^k = A_{iI}x_i^k + B_{iI}u_i^k + \hat{c}_{iI} + diag(\lambda_{iI}^k)^{-1}[\sigma\mu_k e - diag(\tilde{\lambda}_{ai})diag(\tilde{s}_{ai})e]$

where $e = \begin{bmatrix} 1 & 1 & .. & 1 \end{bmatrix}^T$.

Solve the combined predictor-centering–corrector (PCC) direction $(\tilde{z}_p, \tilde{\zeta}_p, \tilde{\lambda}_p, \tilde{s}_p)$ using the method in appendix.

Calculate the scalar

$$\alpha_{\max} = \arg\ \max\{\alpha \in [0,1] \mid \lambda^k + \alpha \tilde{\lambda}_p \geq 0, s^k + \alpha \tilde{s}_p \geq 0\}.$$

Step 4:

Calculate $(z^{k+1}, \xi^{k+1}, \lambda^{k+1}, s^{k+1})$ from equation (3.17)

$$(z^{k+1}, \xi^{k+1}, \lambda^{k+1}, s^{k+1}) = (z^{k+1}, \xi^{k+1}, \lambda^{k+1}, s^{k+1}) + \alpha(\tilde{z}_p, \tilde{\zeta}_p, \tilde{\lambda}_p, \tilde{s}_p) \tag{3.17}$$

where $\alpha = \min(0.995\alpha_{\max}, 1)$.

Then set $k \leftarrow k+1$ and return to step 1.

Step 5:

Calculate the optimal solution

$$u_i^* = u_i^k + \tilde{u}_i\ ,\ x_1^* = x_1^k + \tilde{x}_1\ .$$

Calculate all state variables by using the equation (3.18)

$$x_{i+1}^* = A_i x_i^* + B_i u_i^* \quad \text{for } i=2,...,N-1. \tag{3.18}$$

End: Plot all solutions.

The flowchart of the whole procedures is as follow in Fig. 3.2:

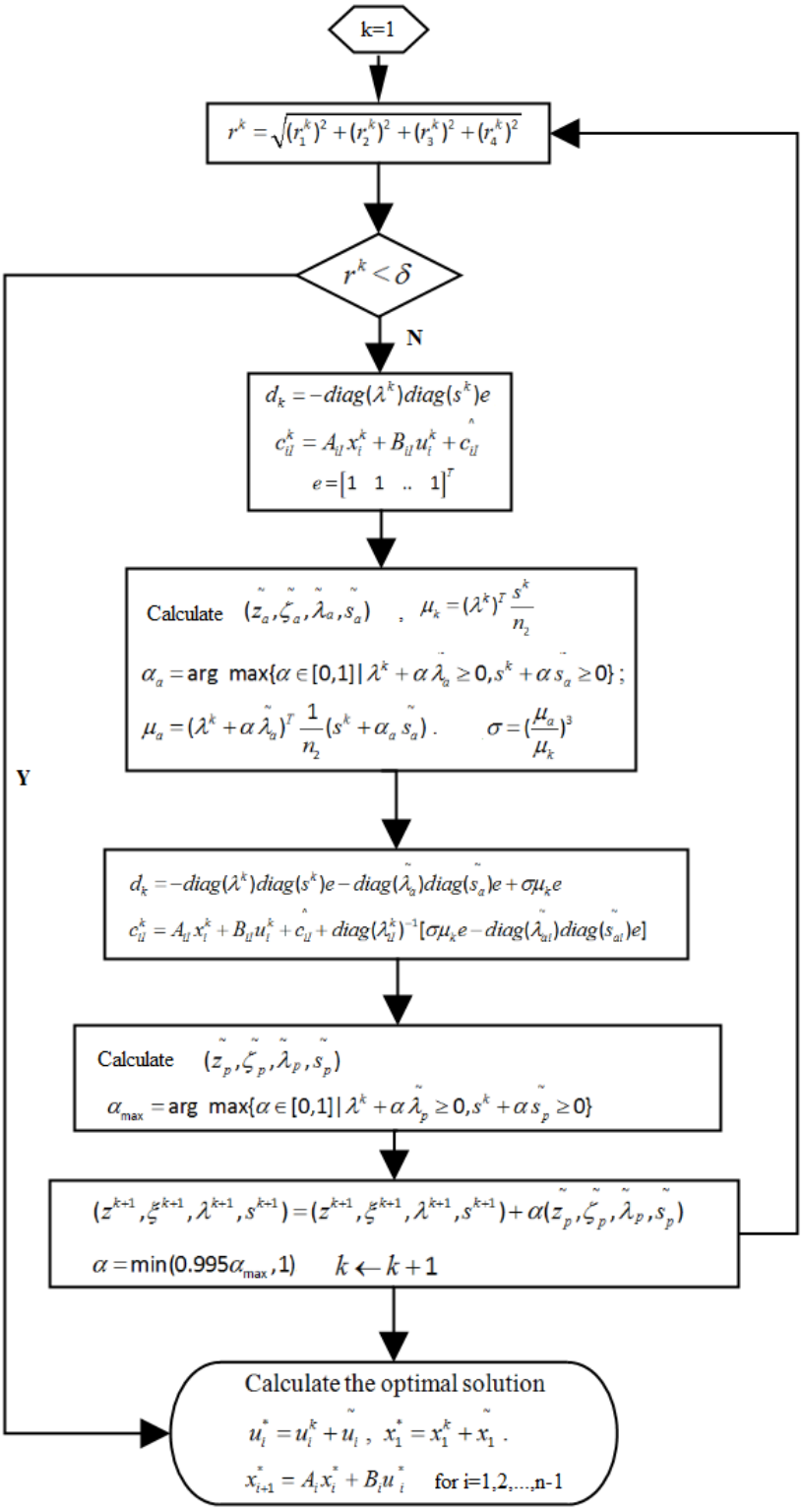

Fig.3.2 Flowchart of the algorithm

3.4 Case Study

A microgrid benchmark [31] shown in Fig. 3.3 is tested in this research. The voltage rating of this microgrid is 400 V. The microgrid is connected to a 20 kv grid through the point of common coupling (PCC) and a transformer.

1) Test case

In this microgrid network, the DERs include the microturbine, fuel cell, wind turbine, photovoltaic, battery and the loads.

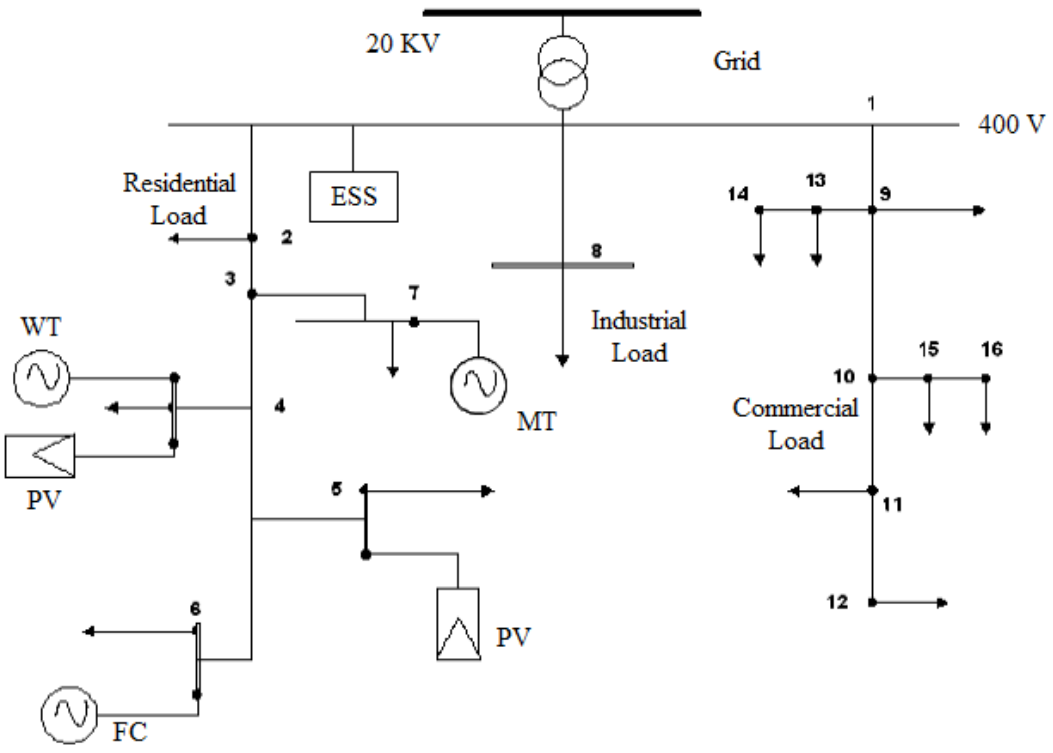

Fig.3.3 Test Case

The parameters of the distributed generation in this microgrid are given in the following tables.

TABLE 3.1 Installed Distributed Generations

Unit Type	Min Power (kW)	Max Power (kW)
MT	6	30
FC	6	50
WT	0	15
PV	0	13
ESS	-30	30

TABLE 3.2 Cost Function Parameters of DGs

Unit Type	b (Ect/kWh)	c (Ect/kWh)	Startup cost
MT	4.37	85.06	9
FC	2.84	255.18	16

TABLE 3.3 Gas Emission Parameters of DGs

Emission Type	Externality cost ($/lb)	Fuel Cell Emission (lb/MWh)	Microturbine Emission (lb/MWh)
CO2	0.014	1.078	1.596
SO2	0.99	0.006	0.008
NOx	4.2	0.03	0.44

The forecasted wind and solar generations are shown in Fig. 3.4.

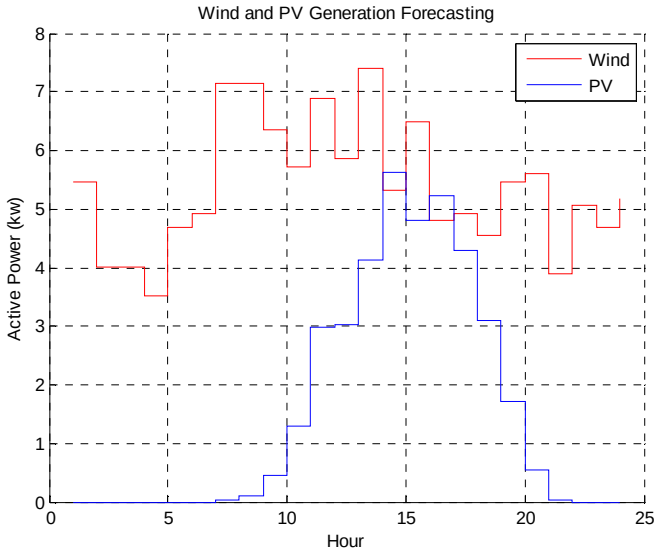

Fig.3.4 Forecasted wind and solar generation

The main grid electricity price (Ect/kWh) is shown in Fig. 3.5.

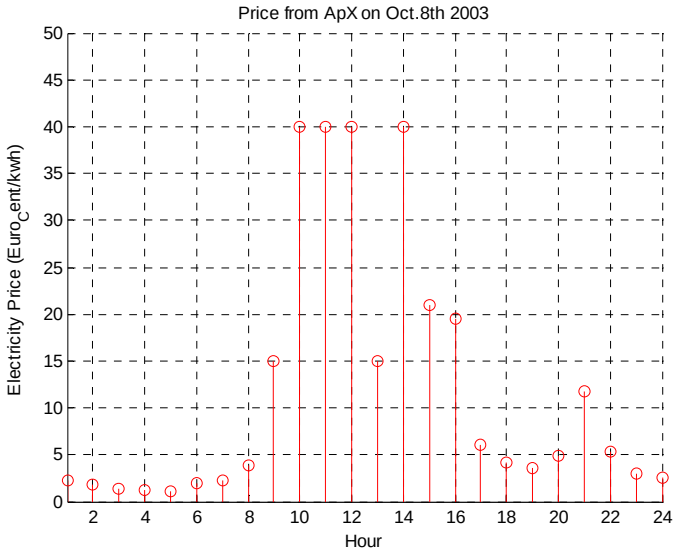

Fig.3.5 Main grid electricity price

2) Operating in stand-alone mode (Policy I)

The load demand for this condition is shown in Fig. 3.6. The maximum load demand is less than the summation of the maximum generation capacity of each unit.

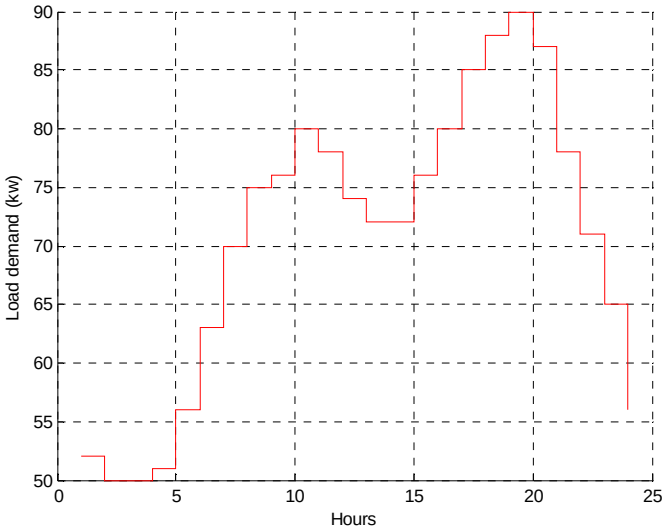

Fig. 3.6 Load demand

The energy scheduling for the next day is shown in Fig. 3.7.

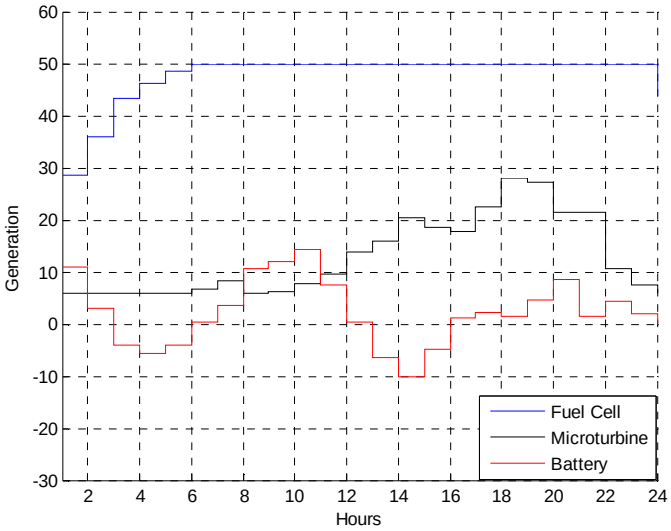

a) Energy scheduling in islanded mode

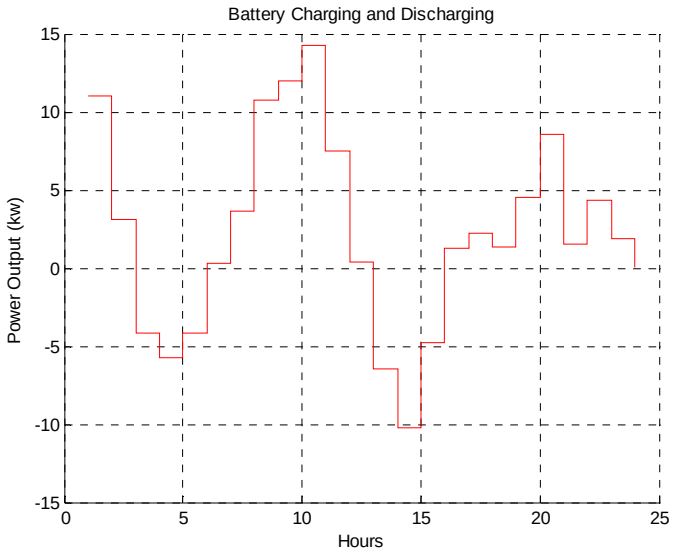

b) Battery charging and discharging

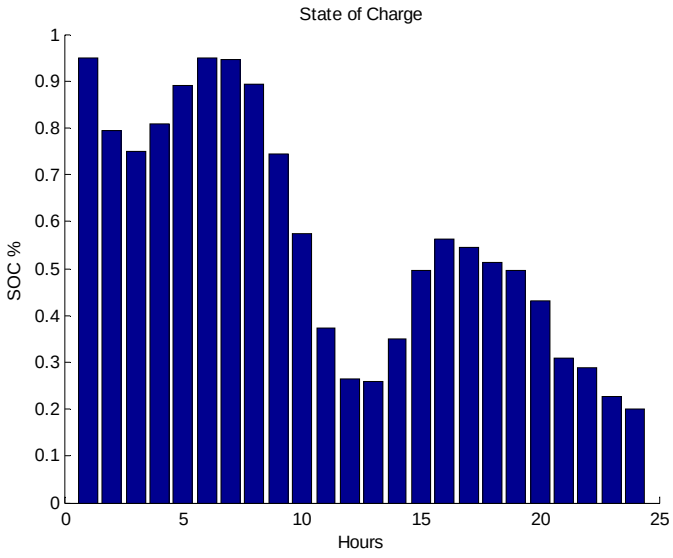

c) Battery SOC

Fig.3.7 a) Energy scheduling during islanded mode; b) Battery charging and discharging; c) Battery SOC.

From the figures shown above, the ESS curve actually has the similar shape as the load curve. When the load is low, the ESS stores energy, most of which comes from the renewable energy resources; while the load demand is high, the ESS sends power to the microgrid and thus reduces the fuel cost.

3) Buy power from main grid (Policy II)

In this case, the microgrid is in a grid-connected mode and receives power from the main grid, thus the load demand is larger than the maximum generation capacity within the microgrid. The load demand curve is shown in Fig. 3.8.

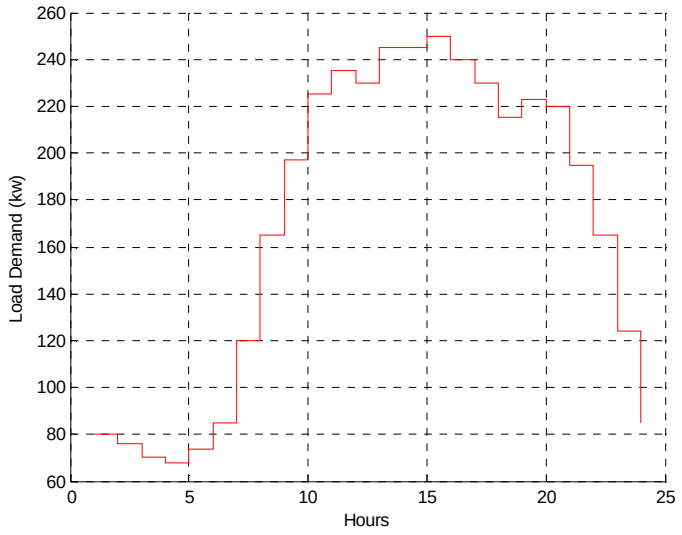

Fig. 3.8 Load demand

The energy scheduling for 24 hours is shown in Fig. 3.9.

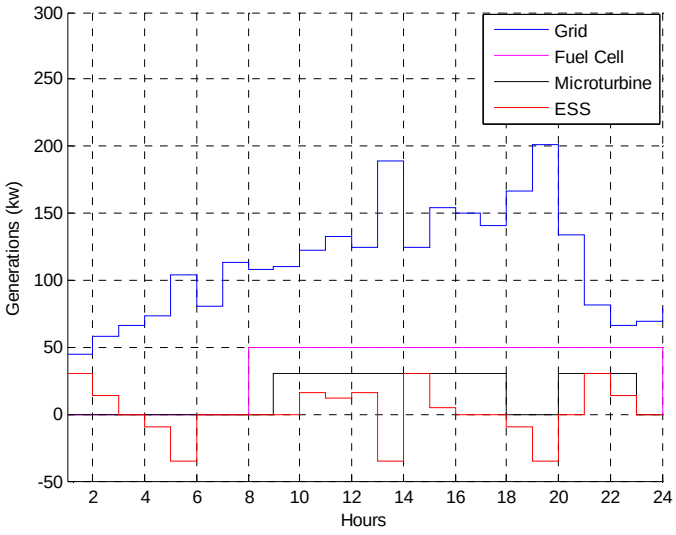

a) Energy scheduling when buying power from main grid

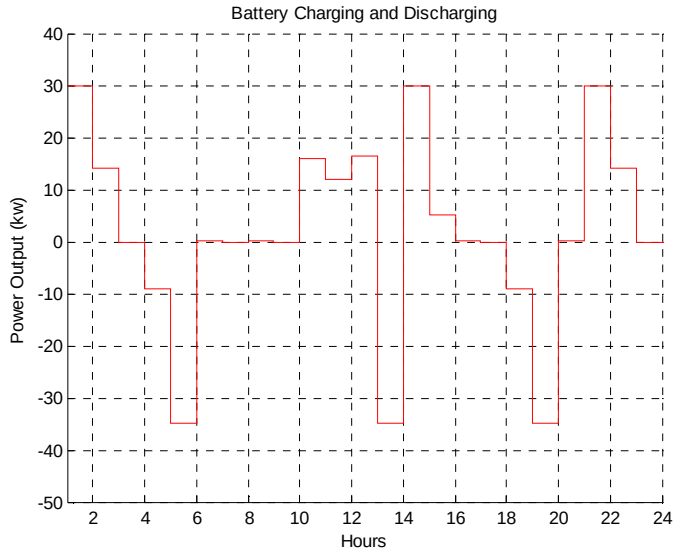

b) Battery charging and discharging

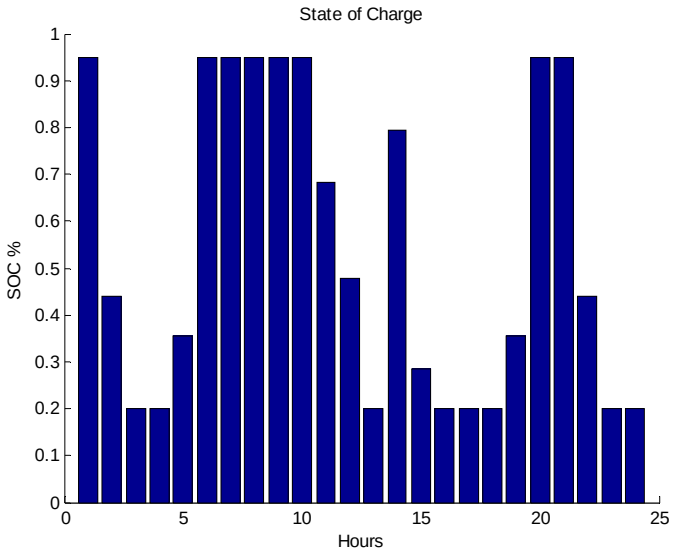

c) Battery SOC

Fig.3.9 a) Energy scheduling when buying power from the main grid; b) Battery charging and discharging; c) Battery SOC.

From Fig. 3.9-b), it appears that the ESS stores energy bought from the main grid when the electricity price is low (3 am to 6 am; 1 pm; and 5pm to 8 pm), and consumes the stored energy within the microgrid when the electricity price in main grid is high (9 am to 12 pm; 2 pm to 3pm; and 9 pm). Hence, the ESS is able to store the cheap energy and discharge it when the energy in main grid is expensive, thus reduces the total cost.

4) Sell power to main grid (Policy II)

The load demand for this condition is shown in Fig. 3.10. The generation within the microgrid is larger than the load demand during some period in a day.

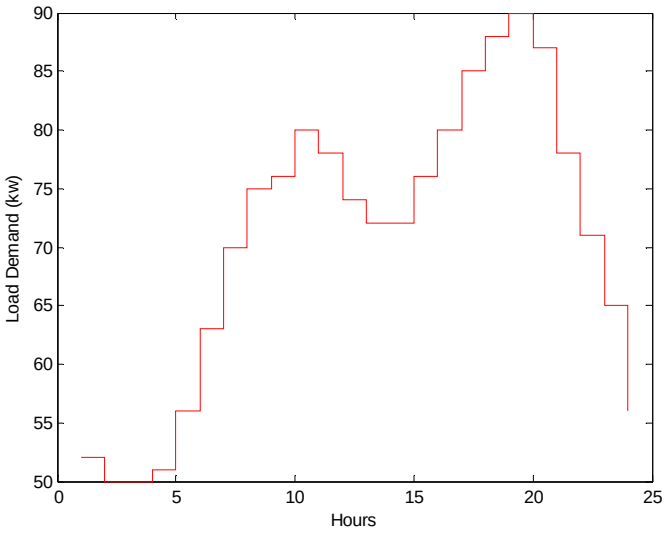

Fig. 3.10 Load demand

The energy scheduling for 24 hours is shown in Fig. 3.11.

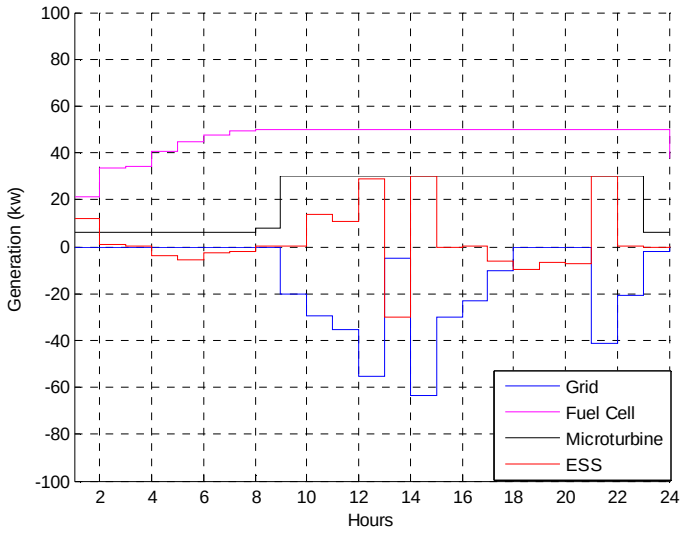

a) Energy scheduling when selling power to main grid

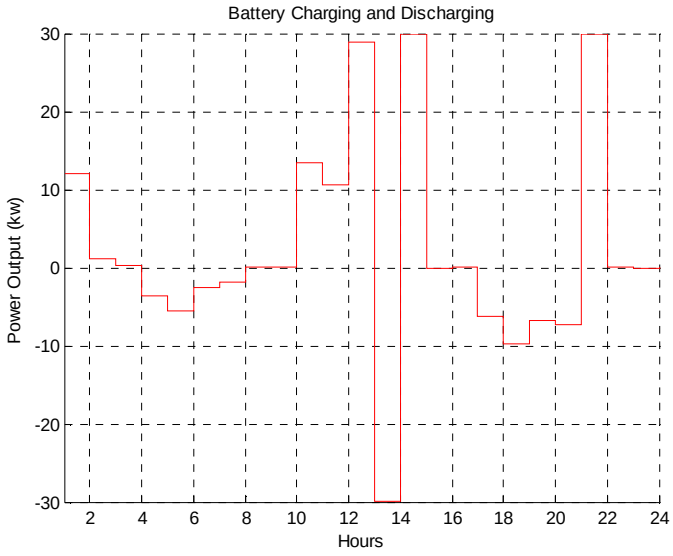

b) Battery charging and discharging

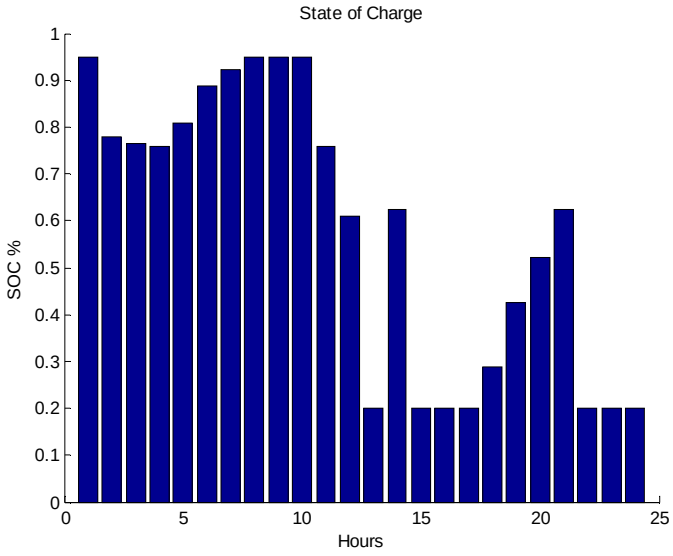

c) Battery SOC.

Fig.3.11 a) Energy scheduling when selling power to main grid; b) Battery charging and discharging; c) Battery SOC.

It can be seen from the above figures that the ESS stores energy when the electricity price in main grid is low (2 am to 9 am; 1 pm; and 5pm to 8 pm), while discharges energy and sends to the main grid when the electricity price is high (10 am to 12 pm; 2 pm to 4pm; and 9 pm). Indeed, the performance of ESS helps the microgrid maximize the profits.

CHAPTER FOUR

CONSIDERATION OF BATTERY LIFE IN OPTIMIZATION MODEL

In a microgrid, it is shown in Chapter Three that the coordination of a battery and other distributed energy resources is able to improve energy utilization efficiency and reduce fuel cost. To maximize the energy utilization efficiency and obtain the optimal solution, the battery may be required to frequently charge or discharge power with a high current rate. However, according to [32], the over-use of a battery will affect its lifetime cycles and damage the battery quickly. Hence, in this chapter the life prediction method of a battery is first studied, and then the factors influencing the battery life will be considered in the optimal energy management model. The model is also solved by the ADP method. At last, the results are presented and compared with the formal results without consideration of battery life.

4.1 Battery Life Prediction Method

According to references [33-35], corrosion is a main component affecting the battery life. Corrosion in battery occurs when Pb in the negative side is oxidized into PbO and PbO_2, which leads to a lower conductivity and higher resistive losses. Actually, multiple factors contribute to the corrosion for a battery, such as the depth of charge, discharge current rate, temperature, battery maintenance procedures, overcharge frequency, current ripple and so on [34]. Among these factors, the depth of charge and discharge current rate are directly related to the energy dispatching in a microgrid in

order to meet the load demand or store system extra power, while other factors are relatively not important in the energy dispatching model. Thus, in this battery life prediction method, the depth of charge and discharge current rate are considered and modeled as two main causes resulting in battery corrosion.

According to the battery life prediction proposed by Symons [36], three premises are given as follows.

Premise 1:

The rated charge life Γ_R is expressed as

$$\Gamma_R = L_R D_R C_R \tag{4.1}$$

where

C_R : Rated amp-hour capacity at rated discharge current I_R;

D_R : Depth of discharge for which rated cycle life was determined, the value equals to (1-soc%);

L_R : Cycle life at rated depth of discharge D_R and discharge current I_R.

Premise 2:

The actual charge life is a function of the depth of discharge. If the battery always discharges power in a large depth, it will decrease the charge life of battery. Thus, the charge life of battery and the depth of discharge have an inverse relation.

Premise 3:

The actual charge life is a function of the discharge rate. If the battery is always in a high discharge rate, it will reduce the charge life of battery. So, the charge life of battery and the depth also have an inverse relation.

Based on the three premises concluded above, experiments are carried out by National Renewable Energy Lab (NREL) [33], and the effect related to the depth of discharge and discharge rate are formulated in the following equations.

1) Influence of depth of discharge

The influence of depth of discharge is calculated in each discharge cycle. In this research, it is assumed that each cycle is an hour. The actual amp-hour discharge in each cycle is the measured amp-hour discharge, while the effective amp-hour discharge means the equivalent discharge subtracted from the amp-hour capacity. Based on the experiment, the relation between the battery cycle life and depth of discharge can be fit using the following equation, and the curve is shown in figure 4.1.

$$L = L_R(\frac{D_R}{D})^{u_0} e^{u_1(1-\frac{D}{D_R})}. \tag{4.2}$$

The relation of the effective amp-hour discharge and the actual amp-hour discharge is

$$\frac{d_{eff}}{d_{actual}} = \frac{L_R}{L} \tag{4.3}$$

So, the effective amp-hour discharge in each specific cycle is a product of the actual amp-hour and an effective weighting coefficient.

$$d_{eff} = (\frac{D_A}{D_R})^{u_0} e^{u_1(\frac{D_A}{D_R}-1)} d_{actual} \tag{4.4}$$

where

L : Actual cycle life of a battery;

L_R : Rated cycle life of a battery;

d_{eff} : Effective amp-hour discharge;

d_{actual} : Actual amp-hour discharge;

D_A : Actual depth of discharge;

D_R : Rated depth of discharge;

u_0 , u_1 : Curve fitting parameters.

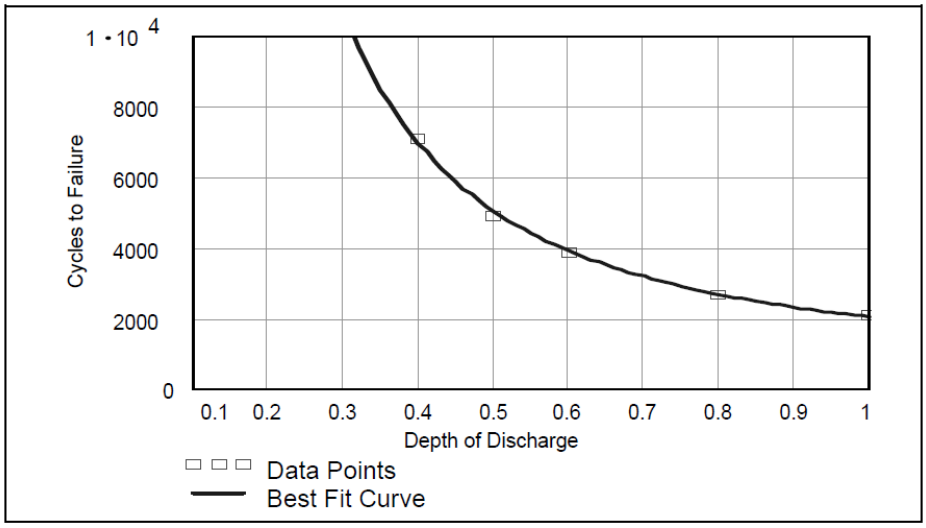

Fig. 4.1 Effect of depth of discharge [33]

2) Influence of discharge rate

According to premise 3, high discharge rate causes low conductivity of a battery and fast the corrosion. Experiment results in Figure 4.2 show the relation between the actual capacity and the discharge rate. The relation between the effective amp-hour discharge and the actual amp-hour discharge is drawn as the following equation.

$$d_{eff} = \frac{C_R}{C_A} d_{actual} \tag{4.5}$$

where

C_R: Rated amp-hour capacity in a rated discharge current;

C_A: Actual amp-hour capacity in a rated discharge current;

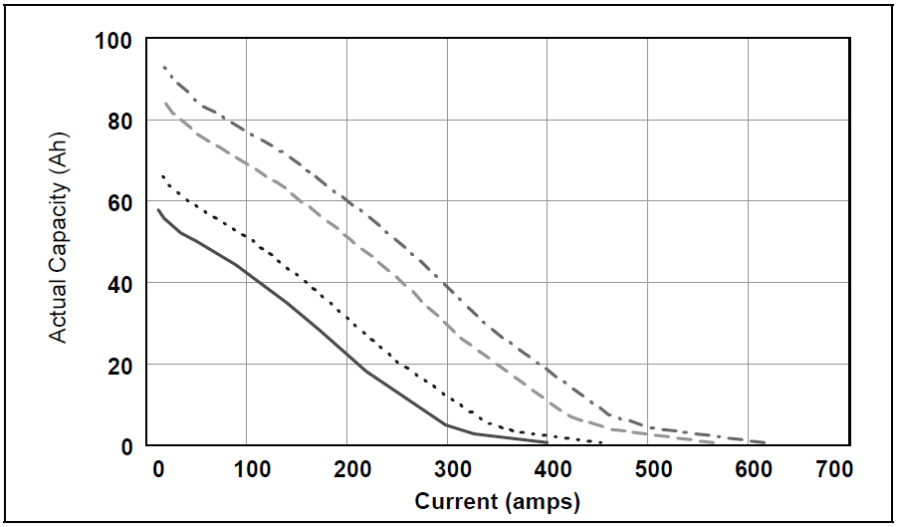

Fig. 4.2 Effect of discharge rate (Four cells with different capacities are tested, they are 58, 67, 85 and 93 amp-hours) [33]

3) Combined influence of both depth of discharge and discharge rate

The effects of depth of discharge and discharge rate are combined by multiplying the factors expressed above, which yields to

$$d_{eff} = \left(\frac{D_A}{D_R}\right)^{u_0} e^{u_1\left(\frac{D_A}{D_R}-1\right)} \frac{C_A}{C_R} d_{actual} \ . \tag{4.6}$$

During time T containing a series of n discharge cycles, the life time L_{time} of the battery under the specified usage pattern is

$$L_{time} = \frac{\Gamma_R}{(\Gamma_{eff} / T)} = \frac{L_R D_R C_R}{\sum_{i=1}^{n} d_{eff}(i)} T \ . \tag{4.7}$$

From the above equation, it can be seen that variables L_R, D_R, C_R and T are constant values. To maximize the battery lifetime, the summation $\sum_{i=1}^{n} d_{eff}(i)$ should be minimized.

4.2 Optimization Model Considering Battery Life

Based on the conclusion in Section 4.1, the summation $\sum_{i=1}^{n} d_{eff}(i)$ should be minimized during a period of time T in order to maximize the battery life. For a day-ahead energy scheduling, the variable n could be 24 and the duration T is 24 hours. Considering the battery life in the optimal energy management model, the effective amp-hour discharge in each interval can be multiplied by a weighting factor and added into the objective function. The value of the weighting factor assigns the significance to each goal in the objective function. Formulations about the objective function are shown as follows.

Objective function without consideration of battery life is

$$\text{Min} \sum_{i=1}^{n} \left(\sum_{j=1}^{m} F_j(P_j(i)) \right); \tag{4.8}$$

Objective function considering battery life is

$$\text{Min} \sum_{i=1}^{n} \left(\lambda \cdot \sum_{j=1}^{m} F_j(P_j(i)) + (1-\lambda) d_{eff}(i) \right); \tag{4.9}$$

or

$$\text{Min} \sum_{i=1}^{n}\left(\sum_{j=1}^{m} F_j(P_j(i)) + (1/\lambda - 1)d_{eff}(i)\right), \tag{4.10}$$

where

i : Time interval series;

j : DG type number;

$F_j(P_j(i))$: Comprehensive costs including the fuel cost and gas emission cost for DG j during interval i;

$d_{eff}(i)$: Effective amp-hour discharge during interval i;

λ : Weighting factor.

The effect amp-hour discharge d_{eff} is

$$d_{eff} = \left(\frac{D_A}{D_R}\right)^{u_0} e^{u_1\left(\frac{D_A}{D_R}-1\right)} \frac{C_R}{C_A} d_{actual} . \tag{4.11}$$

Arrange the expression of d_{eff} and expand the exponential term using Taylor series,

$$d_{eff} = \left(\frac{D_A}{D_R}\right)^{u_0} e^{u_1\left(\frac{D_A}{D_R}-1\right)} \frac{C_R}{C_A} d_{actual}$$

$$= (1-soc)^{u_0} \frac{1}{D_R^{u_0}} e^{u_1} e^{\left(\frac{1-soc}{D_R}-1\right)} \frac{d_R}{d_{actual}} d_{actual} \text{ , the depth of charge } D_A = 1 - soc. \tag{4.12}$$

Since the ratio of the rated and actual discharge capacity is $\frac{C_R}{C_A} = \frac{d_R \cdot t}{d_{actual} \cdot t} = \frac{d_R}{d_{actual}}$, it yields to

$$
\begin{aligned}
d_{eff} &= (1-soc)^{u_0} e^{(\frac{-soc}{D_R})} \frac{e^{(1/D_R-1+u_1)} d_R}{D_R^{u_0}} \\
&= k_0 \cdot (1-u_0 \cdot soc) \cdot (1-soc/D_R) \\
&= k_0 \cdot [1-u_0 \cdot soc + \frac{u_0(u_0-1)}{2} soc^2 + o(soc^2)] \cdot [1-\frac{soc}{D_R} + \frac{soc^2}{2D_R^2} + o(soc^2)] \\
&\approx k_0 \cdot (1-k_1 \cdot soc + k_2 \cdot soc^2)
\end{aligned}
\tag{4.13}
$$

where $k_0 = \frac{d_R e^{(1/D_R+u_1-1)}}{D_R^{u_0}}$, $k_1 = u_0 + \frac{1}{D_R}$, $k_2 = \frac{u_0(u_0-1)}{2} + \frac{u_0}{D_R} + \frac{1}{2D_R^2}$.

It is already known that the state variables in energy management model include $x_1 = P_{grid}$, $x_2 = P_{MT}$, $x_3 = P_{FC}$, $x_4 = P_{Battery}$ and $x_5 = soc$. And according to the parameters given in reference [33] ($u_0 = 0.19$, $u_1 = 1.69$, $d_R = 24$ and $D_R = 0.5$), the values of k_0, k_1 and k_2 are computed as constants. So the effective discharge amp-hour capacity d_{eff} is only a quadratic function about the state variable x_5.

The objective function considering battery life is,

$$
\min \sum_{i=1}^{n} \left(\lambda \cdot \sum_{j=1}^{m} F_j(P_j(i)) + (1-\lambda) d_{eff}(i) \right). \tag{4.14}
$$

Both terms $F_j(P_j(i))$ and $d_{eff}(i)$ are functions about the state variables, the objective function can be combined as equation (4.15):

$$
\min \sum_{i=1}^{n} \left(\sum_{j=1}^{m} F_j^{new}(P_j(i)) \right). \tag{4.15}
$$

where F_j^{new} is the equivalent cost function considering the battery life. The constraints to this objective function are the same as the constraints without consideration of battery life. Finally, the full model is also solved by ADP method.

4.3 Results and Comparisons

In this simulation, the microgrid operates in a stand-alone mode.

1) Without consideration of battery life

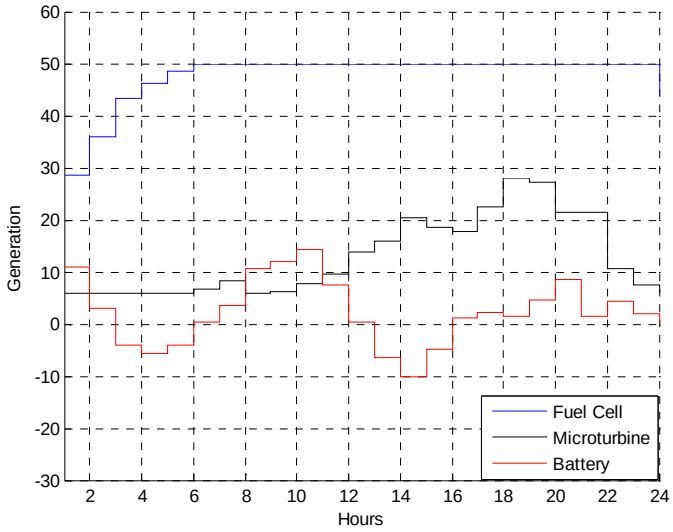

a) Optimal generation dispatching

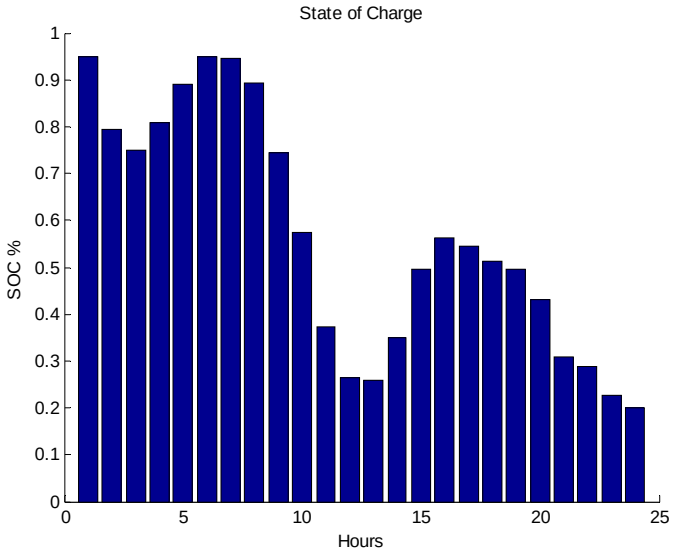

b) Battery state of charge

Fig. 4.3 a) Optimal generation dispatching; b) Battery state of charge.

2) Considering battery life time model, set weighting factor as 0.01.

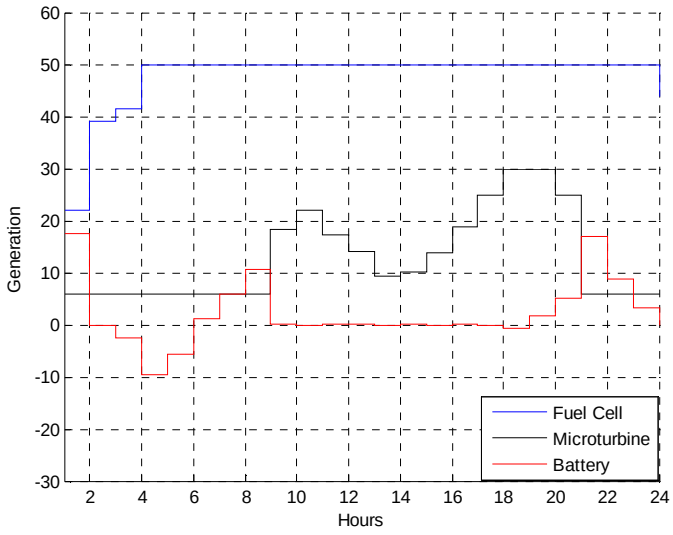

a) Optimal generation dispatching

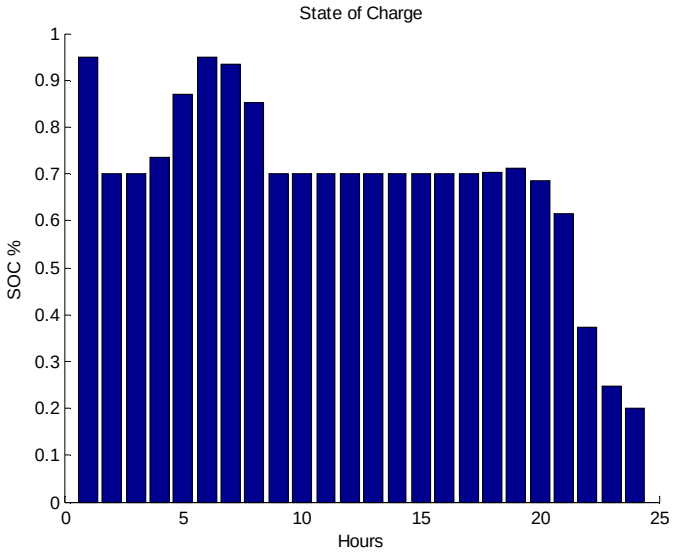

b) Battery state of charge

Fig. 4.4 a) Optimal generation dispatching; b) Battery state of charge

.

c) Comparisons and conclusions:

Figure 4.5 shows the comparison of the battery discharge rate with and without the consideration of battery life.

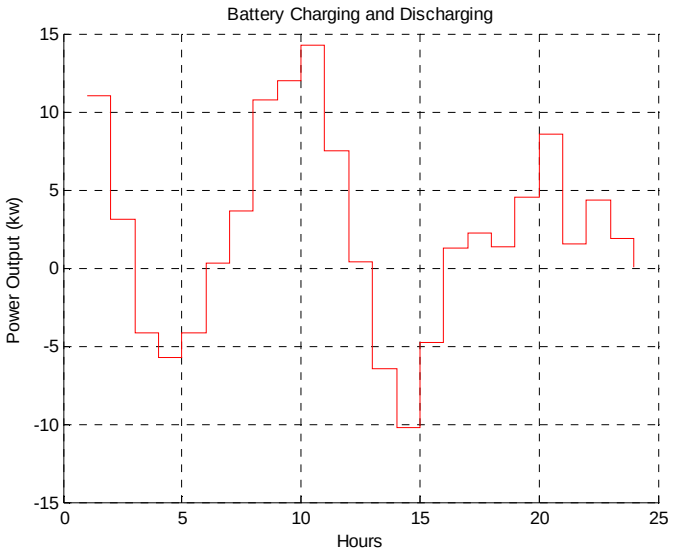

a) Without consideration of battery life

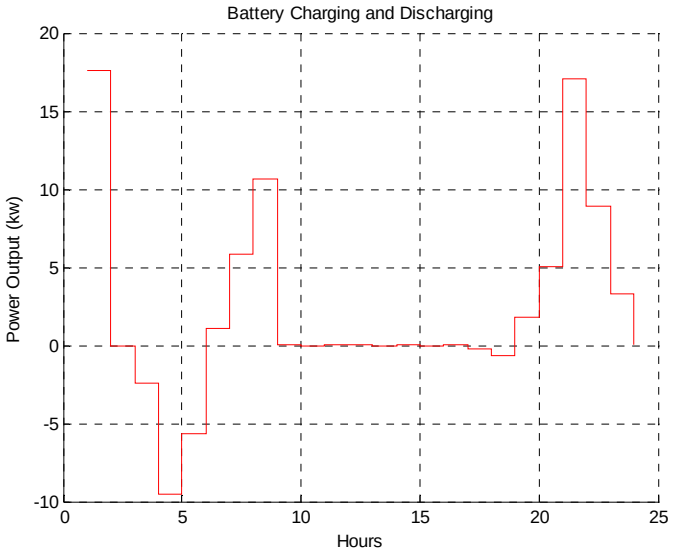

b) Considering battery life

Fig. 4.5 Comparison of battery discharge and charge rate

Figure 4.6 shows the comparison of the battery state of charge with and without the consideration of battery life.

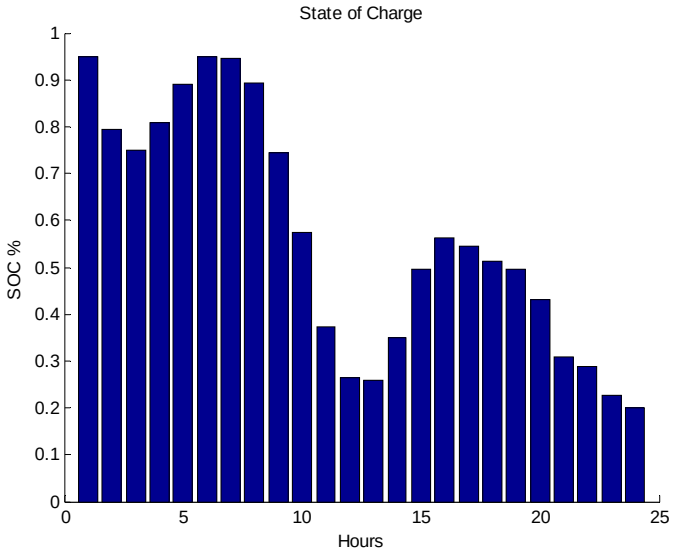

a) Without consideration of battery life

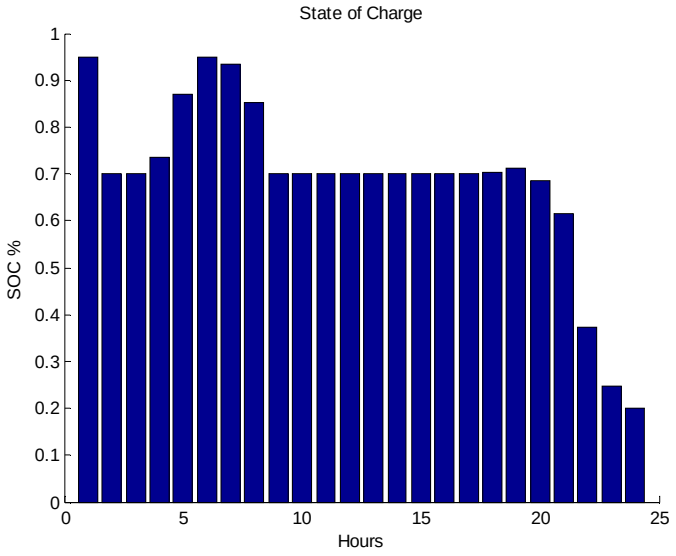

b) Considering battery life

Fig. 4.6 Comparison of battery state of charge

From the above comparisons, it can be seen the battery will operate in a higher level of SOC in average when considering the battery life in the energy management model. During 2:00 am to 6:00 am, the battery stores power from the wind generation; from 7:00 am to 9:00 am when the load is gradually increasing, the battery discharge power; from 10:00 am to 5:00 pm when the solar generation is high, the battery hibernates in order to archive a longer life; during 7:00 pm to midnight when the load demand is high and the solar generation is lost, the battery discharge power.

CHAPTER FIVE

HOURLY OPTIMAL ENERGY SCHEDULING IN MICROGRID

The optimization models shown in chapters three and four work for a day-ahead energy scheduling in microgrid. In previous models, the wind generation is calculated based on the day-ahead wind speed forecasting, the solar generation is estimated by day-ahead solar irradiation and temperature forecasting, and the load curve is forecasted on the basis of the historical load data. In recent years, several references [37-41] have presented the algorithms forecasting the wind generation, solar generation and load demand. However, the events of wind generation, solar generation and load demand are all stochastic processes and affected by many uncertain factors, such as the weather change, social events, accident and so on. Thus, the actual values of the wind generation, solar generation and load in each hour on the next day may vary from the forecasted data due to varying reasons. In this case, an hourly optimal energy scheduling method is proposed in this chapter in order to track the real circumstances and minimize the errors between the scheduled generations and actual generations. The formulation below shows the objective of the hourly energy management in microgrid.

$$\text{Min Error} = \sum_{t=1}^{24}\sum_{j=1}^{m}[P_{j\_scheduled}(t) - P_{j\_actual}(t)]^2 \tag{5.1}$$

Different from the day-ahead energy management model, the hourly energy scheduling is carried out in each hour based on the updated forecasting data of the next 24 hours. The hourly model can be solved by the same ADP algorithm as the day-ahead

model. Since the forecasted wind generation is more likely to be disturbed by the changeable wind speed while the forecasted solar generation and load demand are relatively more stable than the wind generation, without loss of generality, the forecasted wind generations of the next 24 hour are updated in each hour and applied into the hourly model.

5.1 Description of hourly energy management model

The difference between the day-ahead model and hourly model is that the next 24 hours wind generation should be forecasted repeatedly in each hour and the optimization engine is ran in each hour. The wind generation is calculated by the forecasted wind speed, and the forecasted wind speed for the next 24 hours can be accessed instantly from the website resource [42-43].

By solving the optimization problem at each hour, the unit generation schedules for the next 24 hours can be obtained. However, not all schedules of the next 24 hours are useful for power operator. The power operator will be only guided by the schedule of the first hour. For the second hour, the power operator will update the energy dispatching schedule while he gets updated wind generation forecasting in the first hour. This procedure repeats till the last hour during a day. Figure 5.1 shows the diagram of the hourly energy management method.

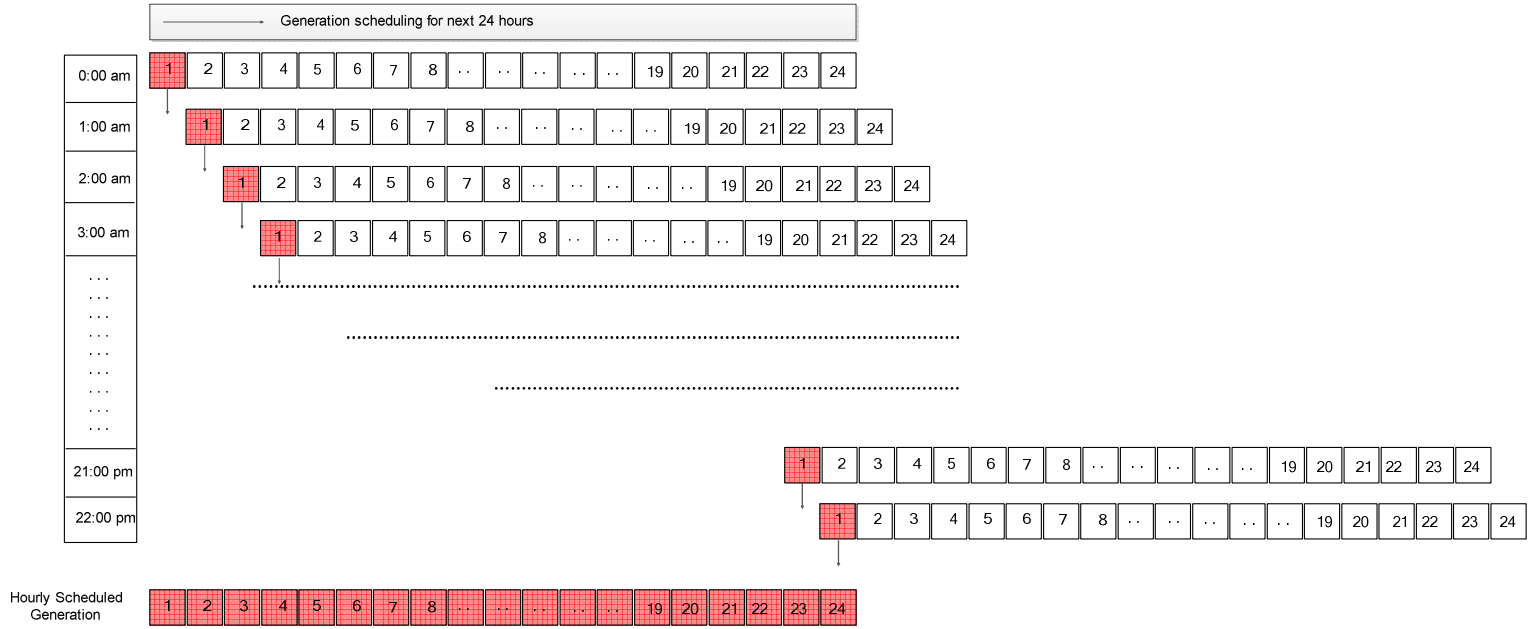

Fig. 5.1 Hourly energy management method

5.2 Simulation results and comparisons

The simulation is carried out on an islanded microgrid operated under policy I.

1) Day-ahead scheduling results

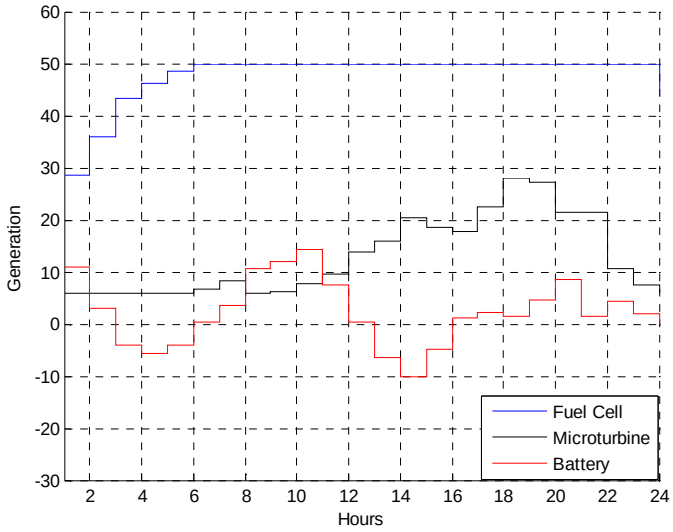

a) Scheduled generation for DERs

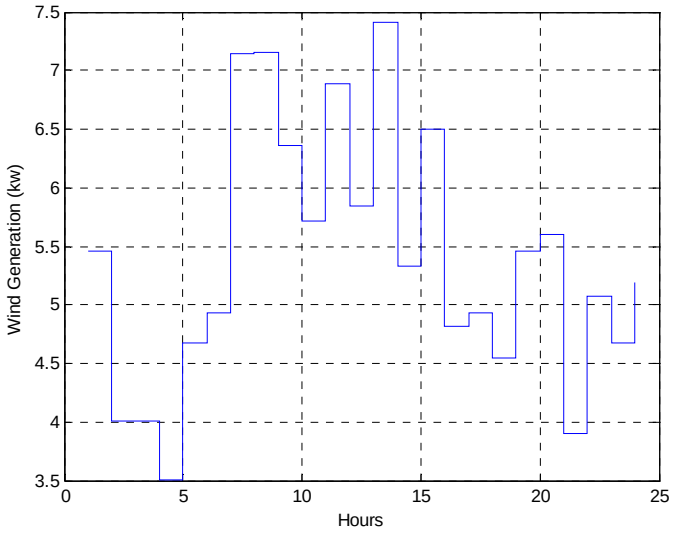

b) Day-ahead forecasted wind generation

Fig. 5.2 Results of day-ahead model

2) Actual circumstance

Here, the actual circumstance means the wind generation used in the model is the actual wind generation. In fact, this is an ideal case.

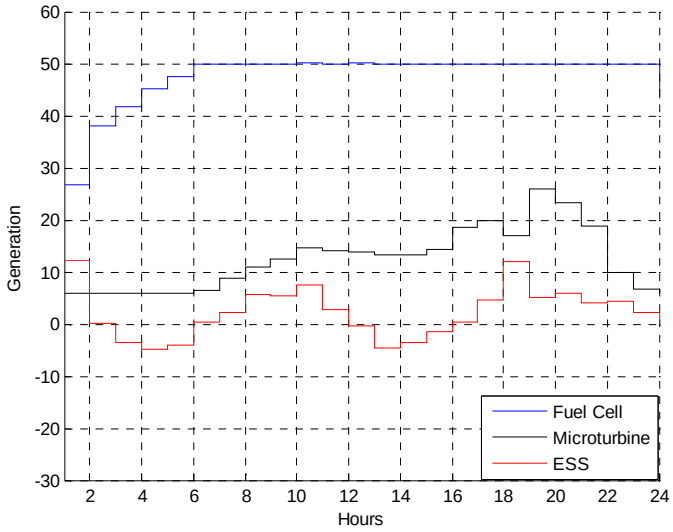

a) Actual geneartion for DERs

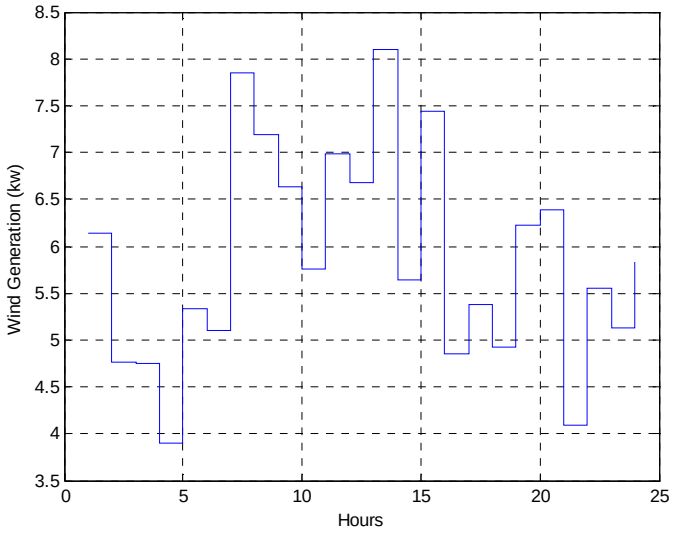

b) Actual wind generation

Fig. 5.3 Actual energy dispatching

3) Hourly scheduling results

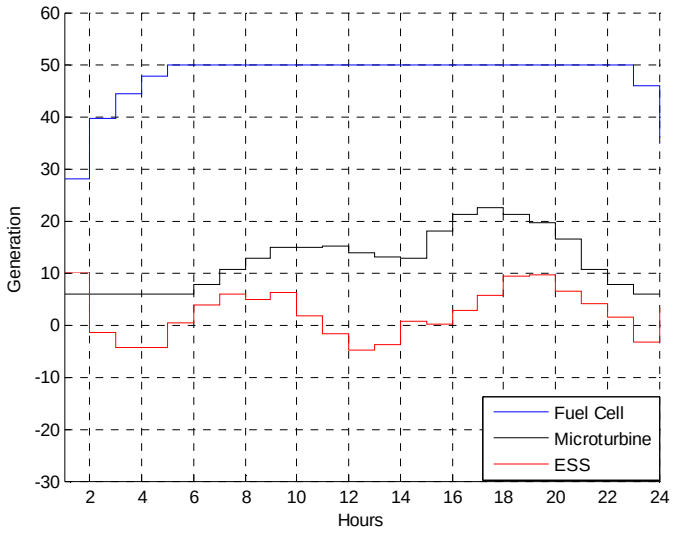

Fig. 5.4 Results of hourly model

4) Comparison of the energy scheduling under three cases

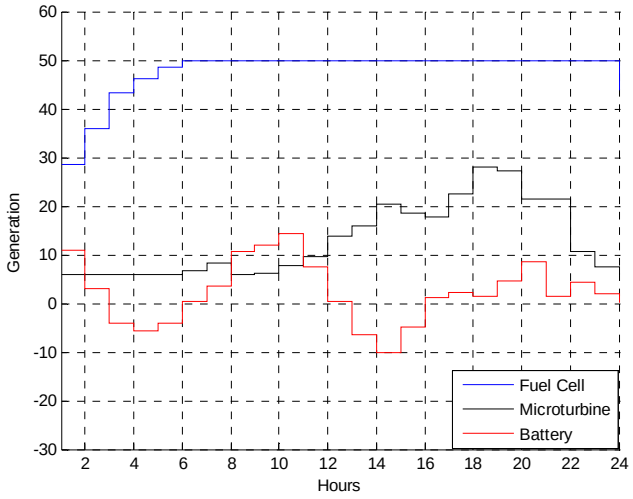

a) Day-ahead model (Error=705.45 kw^2)

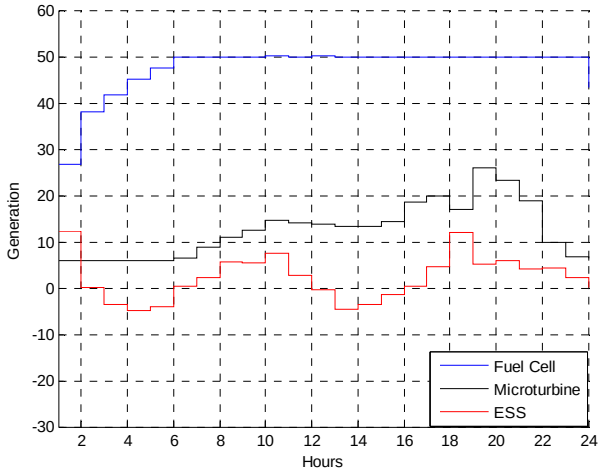

b) Actual circumstance (Error=0 kw^2)

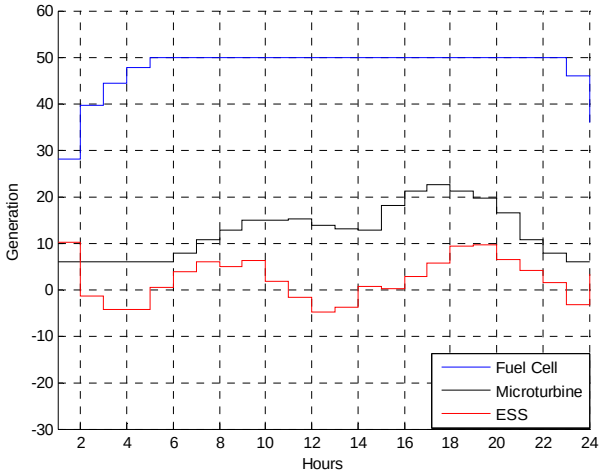

c) Hourly model (Error=542.02 kw^2)

Fig. 5.5 Comparison of energy dispatching curves

It can be observed that the hourly scheduled curves are similar as the actual circumstance. Calculating the error by using equation (5.1), the error for the day-ahead energy scheduling model is 705.4479 while the error for the hourly energy scheduling model is 542.0151.

CHAPTER SIX

CONCLUSIONS

In this thesis, the optimal energy management for a microgrid is studied. The purpose is to plan a generation schedule for each unit in each hour on the next day in order to minimize the fuel cost, reduce gas emissions and improve energy utilization efficiency. The microgrid energy management problem is investigated under both the grid-connected mode and the stand-alone mode. The performance of battery and its coordination with other DERs are well considered in this problem.

Three major contribution of this research are:

1) The ADP algorithm is used to solve the energy management model featured as multi-parametric nonlinear programming constrained by dynamic programming. This algorithm is proved to be efficient and easy to converge.

2) The battery life is considered in the energy management model. It is presented that the depth of discharge and discharge current rate are two main factors influencing the battery life. The save usage pattern of battery is concluded.

3) Track the system variables, the hourly energy management model is also studied using ADP algorithm and considering the dynamic performance of battery.

Simulation results of this research are summarized as follows.

a) Day-ahead energy scheduling model without consideration of battery life

Policy I: The microgrid operates in stand-alone mode. When the system load is low, the battery stores energy, most of which comes from the renewable energy

resources; when the load demand is high, the battery discharges power to the microgrid and releases the generation burden of fuel consumed units.

Policy II (buy power from the main grid): In this case, the microgrid is connected to the main grid and the system load is larger than the system maximum generation capacity. So the microgrid needs to receive power from the main grid. The battery stores energy bought from the main grid when the electricity price is low (3 am to 6 am; 1 pm; and 5pm to 8 pm), and consumes the stored energy within the microgrid when the electricity price in main grid is high (9 am to 12 pm; 2 pm to 3pm; and 9 pm). Hence, the battery is able to store the cheap energy and discharge it when the electricity price in main grid is high, thus reduces the total cost.

Policy II (sell power to the main grid): In this case, the microgrid is connected to the main grid and the system load is less than the maximum generation capacity. So the microgrid will have opportunities selling excess power to the main grid. The battery stores energy when the electricity price in main grid is low (2 am to 9 am; 1 pm; and 5pm to 8 pm), while discharges power to the main grid when the electricity price is high (10 am to 12 pm; 2 pm to 4pm; and 9 pm). Indeed, the performance of ESS helps the microgrid maximize the profits.

b) Day-ahead energy scheduling model considering battery life

From the results and comparisons, it can be seen the battery charging and discharging frequency is reduced in order to maintain a good usage pattern and avoid over-use. During 2:00 am to 6:00 am, the battery stores power from the wind generation; from 7:00 am to 9:00 am when the load is gradually increasing and the solar generation is

low, the battery discharge power; from 10:00 am to 5:00 pm when the solar generation is high, the battery hibernates; during 7:00 pm to midnight when the load demand is high and the solar generation is lost, the battery discharge power.

c) Hourly energy scheduling model

The hourly scheduled curves approach to the curves in actual circumstances. The scheduled error of the hourly model is smaller than the day-ahead model.

In a summary, the ADP algorithm works well for the microgrid energy management problem. It is fast and easy to converge. Without the consideration of battery life, the battery performs much and is able to improve the energy utilization efficiency. When consider the battery life in the model, the performance of battery is limited and the save usage pattern of battery can be achieved.

APPENDICES

Appendix A

Code for Energy Management Optimization

The following code applies to policy one that the microgrid is in a stand-alone mode.

```
clc;
clear;
%Algorithm Parameters
f=0;
k=1;
ef=0.8;
n=24;
nx=5;
nu=4;
% Diesel Engine
c_de=0.7323*1.03*100; %eurocent/L
a=0.4333;
b=0.2333;
c=0.0074;
p1min=1; %kW
p1max=6;
% Fuel cell
% c_fc=0.0164; %dollar/kwh
% oper_fc=3.68; %dollar/h
% effi_fc=0.4;
p2min=3;
p2max=50;
% Microturbine
% c_mt=0.0164;
% effi_mt=0.26;
% oper_mt=1.228;
p3min=6;
p3max=30;
% ESS
ef=0.85;
wmax=60;
p4min=-30;
p4max=30;
% SOC Limits
p5min=0.2;
p5max=0.95;
k1=c_de*c;
k2=2.84;
k3=4.37;
k4=c_de*b;
beta=0.05;
PvMax=13;
PwtMax=15;
```

```
Pl=[52 50 50 51 56 63 70 75 76 80 78 74 72 72 76 80 85 88 90 87 78 71
65 56];
Pv=[0 0 0 0 0 0 0.002 0.008 0.035 0.1 0.23 0.233 0.318 0.433 0.37 0.403
0.33 0.238 0.133 0.043 0.003 0 0 0]*PvMax;
Pwt=[0.364 0.267 0.267 0.234 0.312 0.329 0.476 0.477 0.424 0.381 0.459
0.390 0.494 0.355 0.433 0.321 0.329 0.303 0.364 0.373 0.260 0.338 0.312
0.346]*PwtMax;
Ai=[1 0 0 0 0;
     0 1 0 0 0;
     0 0 1 0 0;
     0 0 0 1 0;
     0 0 0 -ef/wmax 1];
 Bi=[1 0 0 0;
     0 1 0 0;
     0 0 1 0;
     0 0 0 1;
     0 0 0 0];
 AiE=[1 1 1 1 0];
 BiE(1,1:4)=0;
 AiI=[1 0 0 0 0;
     -1 0 0 0 0;
      1 0 0 0 0;
     -1 0 0 0 0;
     0 1 0 0 0;
     0 -1 0 0 0;
     0 1 0 0 0;
     0 -1 0 0 0;
     0 0 1 0 0;
     0 0 -1 0 0;
     0 0 1 0 0;
     0 0 -1 0 0;
     0 0 0 1 0;
     0 0 0 -1 0;
     0 0 0 1 0;
     0 0 0 -1 0;
     0 0 0 0 1;
     0 0 0 0 -1;
     0 0 0 -ef/wmax 1;
     0 0 0 ef/wmax -1;
     ];
  n_ieq=length(AiI(:,1));
  BiI(1:n_ieq,1:4)=[0 0 0 0;
                    0 0 0 0;
                    1 0 0 0;
                   -1 0 0 0;
                   0 0 0 0;
                    0 0 0 0;
                    0 1 0 0;
                    0 -1 0 0;
                    0 0 0 0;
                    0 0 0 0;
                    0 0 1 0;
                    0 0 -1 0;
                    0 0 0 0;
```

```
                0 0 0 0;
                0 0 0 1;
                0 0 0 -1;
                0 0 0 0;
                0 0 0 0;
                0 0 0 0;
                0 0 0 0;
               ];
      Qi=[2*k4 0 0 0 0;
           0 0 0 0 0;
           0 0 0 0 0;
           0 0 0 0 0;
           0 0 0 0 0];
    Ri=0;
    Si=0;
    yi=[k1;k2;k3;0;0];
    zi=0;
    e(1:(24*n_ieq),1)=1;
    ei(1:n_ieq,1)=1;
    n2=n_ieq*n;
    cmax=10000;
    epz=0.01;
    theta=0.00001;
    u(1:4,1:23,k)=0;
    x(1:5,1,k)=0;
    lamdiE(1,1:n,k)=0.01;
    for i1=1:n
        if i1>1
         x(1:5,i1,k)=Ai*x(:,i1-1,k)+Bi*u(:,i1-1,k);
        end
        lamdiI(1:n_ieq,i1,k)=epz*ei;
        cpp=[-p1max;p1min;-p1max;p1min;-p2max;p2min;-p2max;p2min;-
p3max;p3min;-p3max;p3min;-p4max;p4min;-p4max;p4min;-p5max;p5min;-
p5max;p5min];
        siI(1:n_ieq,i1,k)=max(-cpp,epz*ei);
    end
while f>-1
  for loop=1:2
  r1k2=0;r2k2=0;r3k2=0;r4k2=0;
  for i=n:-1:1
    ciE=-(Pl(i)-Pv(i)-Pwt(i));
    ciI=[-p1max;p1min;-p1max;p1min;-p2max;p2min;-p2max;p2min;-
p3max;p3min;-p3max;p3min;-p4max;p4min;-p4max;p4min;-p5max;p5min;-
p5max;p5min];
    ciEa(1,i)=ciE;
    ciIa(1:n_ieq,i)=ciI;
    yik=yi+Qi*x(:,i,k)+AiE'*lamdiE(:,i,k)+AiI'*lamdiI(:,i,k);
    zik=zi+BiI'*lamdiI(:,i,k);
    ciEk=AiE*x(:,i,k)+ciE;
    Sik=0;Lik=0;
      for i0=1:n_ieq
          Lik(i0,i0)=lamdiI(i0,i,k);
          Sik(i0,i0)=siI(i0,i,k);
      end
```

```
    if loop==1
          dik=-Lik*Sik*ei;
          if i==n
            ciIk=AiI*x(:,i,k)+ciI;
          else
            ciIk=AiI*x(:,i,k)+BiI*u(:,i,k)+ciI;
          end
          ciIka(:,i)=ciIk;

    else
         dik=-Lik*Sik*ei-Lika(:,:,i)*Sika(:,:,i)*ei+zeta*miuk*ei;
          if i==n
             ciIk=AiI*x(:,i,k)+ciI+inv(Lik)*(zeta*miuk*ei-
Lika(:,:,i)*Sika(:,:,i)*ei);
          else
             ciIk=AiI*x(:,i,k)+BiI*u(:,i,k)+ciI+inv(Lik)*dik+Sik*ei;
          end
          ciIka(:,i)=ciIk;
    end
    Gik=inv(Lik)*(Sik);
    len=length(Gik(:,1));
    [eix,eiv]=eig(Gik);
    eivv(1:len,1:len)=0;
    eivv=eiv;
    pr=eix;
    pc=eix';
    p=pr;
    for ii=1:len
        if (ii==1) & (eivv(ii,ii)>1 | eivv(ii,ii)==1)
            Pib=0;
            Pif=p(:,1:len);
            Gib=0;
            Gif=eivv(1:len,1:len);
            Pi_hat=Pif*inv(Gif)*Pif';
            yi_hat=yik+AiI'*Pi_hat*ciIk;
            zi_hat=zik+BiI'*Pi_hat*ciIk;
            Qi_hat=Qi+AiI'*Pi_hat*AiI;
            Ri_hat=AiI'*Pi_hat*BiI;
            Si_hat=BiI'*Pi_hat*BiI;
            Ai_hat=AiE;
            Bi_hat=BiE;
            ci_hat=ciEk;
            br=0;
            Gi_hat(1:AiE(:,1),1:AiE(:,1))=0;
            lenG_r=1;
            lenG_c=1;
            lenpib(i)=0;
            break;
        end
        if (ii==len)& (eivv(ii,ii)<1)
            Pib=p(:,1:len);
            Pif=0;
            Gib=eivv(1:len,1:len);
```

```
            Gif=0;
            Pi_hat=0;
            yi_hat=yik;
            zi_hat=zik;
            Qi_hat=Qi;
            Ri_hat=0;
            Si_hat=0;
            Ai_hat=[AiE;Pib'*AiI];
            Bi_hat=[BiE;Pib'*BiI];
            ci_hat=[ciEk;Pib'*ciIk];
            br=len-1;
            Gi_hat(1:AiE(:,1),1:AiE(:,1))=0;

Gi_hat((AiE(:,1)+1):(AiE(:,1)+length(Gib(:,1))),(AiE(:,1)+1):(AiE(:,1)+
length(Gib(:,1))))=Gib;
            lenG_r=1+len;
            lenG_c=1+len;
            lenpib(i)=len;
            break;
        end
        if (ii>1) & (eivv(ii,ii)>1 | eivv(ii,ii)==1)
            br=ii-1;
            Pib=p(:,1:br);
            Pif=p(:,(br+1):len);
            Gib=eivv(1:br,1:br);
            Gif=eivv((br+1):len,(br+1):len);
            Pi_hat=Pif*inv(Gif)*Pif';
            yi_hat=yik+AiI'*Pi_hat*ciIk;
            zi_hat=zik+BiI'*Pi_hat*ciIk;
            Qi_hat=Qi+AiI'*Pi_hat*AiI;
            Ri_hat=AiI'*Pi_hat*BiI;
            Si_hat=BiI'*Pi_hat*BiI;
            Ai_hat=[AiE;Pib'*AiI];
            Bi_hat=[BiE;Pib'*BiI];
            ci_hat=[ciEk;Pib'*ciIk];
            Gi_hat(1:AiE(:,1),1:AiE(:,1))=0;

Gi_hat((AiE(:,1)+1):(AiE(:,1)+length(Gib(:,1))),(AiE(:,1)+1):(AiE(:,1)+
length(Gib(:,1))))=Gib;
            lenG_r=1+br;
            lenG_c=1+br;
            lenpib(i)=br;
            break;
        end
    end
    if Gif==0
      mm2=0;
      lenmm2_r(i)=0;
      lenmm2_c(i)=0;
      cof2(1,1,i)=0;
    else
      mm2=Pif*inv(Gif)*Pif';
      lenmm2_r(i)=length(mm2(:,1));
      lenmm2_c(i)=length(mm2(1,:));
```

```
      cof2(1:lenmm2_r(i),1:lenmm2_c(i),i)=mm2;
    end
    if Pib==0
    mm1=Pib;
    lenmm1_r(i)=0;
    lenmm1_c(i)=0;
    cof1(1,1,i)=mm1;
    else
    mm1=Pib;
    lenmm1_r(i)=length(mm1(:,1));
    lenmm1_c(i)=length(mm1(1,:));
    cof1(1:lenmm1_r(i),1:lenmm1_c(i),i)=mm1;
    end
    if i==n
        lenAi_c=length(Ai_hat(1,:));
        lenAi_r=length(Ai_hat(:,1));
        lenBi_c=lenG_c;
        lenBi_r=lenG_r;
        lenCn=length(ci_hat(:,1));
        A(1:length(Ai_hat(:,1)),1:length(Ai_hat(1,:)),i)=Ai_hat;
        B(1:lenBi_r,1:lenBi_c,i)=-Gi_hat(1:lenG_r,1:lenG_c);
        cn(1:lenCn,i)=ci_hat;
        v(1:nx,i)=yi_hat;
        W(1:length(Qi_hat(:,1)),1:length(Qi_hat(1,:)),i)=Qi_hat;
        c(1:length(yi_hat),i)=yi_hat;
        r2k2=r2k2+(AiE*x(:,i,k)+ciE)'*(AiE*x(:,i,k)+ciE);

r3k2=r3k2+(AiI*x(:,i,k)+ciI+siI(:,i,k))'*(AiI*x(:,i,k)+ciI+siI(:,i,k));
r4k2=r4k2+min(lamdiI(:,i,k),siI(:,i,k))'*min(lamdiI(:,i,k),siI(:,i,k));
        continue;
    end
    H1i=Qi_hat+Ai'*W(:,:,i+1)*Ai;
    H2i=Ri_hat+Ai'*W(:,:,i+1)*Bi;
    H3i=Si_hat+Bi'*W(:,:,i+1)*Bi;
    h4i=yi_hat+Ai'*v(1:nx,i+1);
    h5i=zi_hat+Bi'*v(1:nx,i+1);
    zero1(1:length(Bi_hat(:,1)),1:lenBi_c)=0;
    zero2(1:lenBi_r,1:lenG_c)=0;
    F1i=[H3i Bi_hat' Bi'*A(1:lenAi_r,1:lenAi_c,i+1)';
         Bi_hat -Gi_hat(1:lenG_r,1:lenG_c)
zero1(1:length(Bi_hat(:,1)),1:lenBi_c);
         A(1:lenAi_r,1:lenAi_c,i+1)*Bi zero2(1:lenBi_r,1:lenG_c)
B(1:lenBi_r,1:lenBi_c,i+1)];
    F2i=[H2i';Ai_hat;A(1:lenAi_r,1:lenAi_c,i+1)*Ai];
    f3i=[h5i;ci_hat;cn(1:lenCn,i+1)];
    len1=length(F1i(:,1));
    [u_F,s_F,v_F]=svd(F1i);
    for jj=2:len1
        if s_F(jj,jj)/s_F(1,1)<1/cmax
           maxj=jj-1;
           break;
        end
    end
    nir=max(maxj,len1-n);
```

```
    nin=len1-nir;
    ipzi(1:len1,1:len1)=u_F'*F1i*u_F;
    ipzir=0;ipzin=0;
    ipzir=ipzi(1:nir,1:nir);
    ipzin=ipzi((nir+1):len1,(nir+1):len1);
    phir=u_F(:,1:nir);
    phin=u_F(:,(nir+1):len1);
    phi=u_F;
    cc1=phin'*F2i;
    cc2=ipzin;
    cc3=phin'*f3i;
    lenAi_c=length(cc1(1,:));
    lenAi_r=length(cc1(:,1));
    lenBi_c=length(cc2(1,:));
    lenBi_r=length(cc2(:,1));
    lenCn=length(cc3(:,1));
    A(1:lenAi_r,1:lenAi_c,i)=phin'*F2i;
    B(1:lenBi_r,1:lenBi_c,i)=ipzin;
    cn(1:lenCn,i)=phin'*f3i;
    cc4=inv(ipzir)*phir'*F2i;
    cc5=inv(ipzir)*phir'*f3i;
    lenE1i_r(i)=length(cc4(:,1));
    lenE1i_c(i)=length(cc4(1,:));
    lene2i_r(i)=length(cc5(:,1));
    lene2i_c(i)=length(cc5(1,:));
    E1i(1:lenE1i_r(i),1:lenE1i_c(i),i)=inv(ipzir)*phir'*F2i;
    e2i(1:lene2i_r(i),1:lene2i_c(i),i)=inv(ipzir)*phir'*f3i;
    W(:,:,i)=H1i-F2i'*phir*E1i(1:lenE1i_r(i),1:lenE1i_c(i),i);
    v(:,i)=h4i-F2i'*phir*e2i(1:lene2i_r(i),1:lene2i_c(i),i);
    lenphi_r(i)=length(phi(:,1));
    phistore(1:lenphi_r(i),1:lenphi_r(i),i)=phi;
    c(:,i)=yi_hat+Ai'*c(:,i+1);
    r1k2=r1k2+(zi_hat+Bi'*c(:,i))'*(zi_hat+Bi'*c(:,i));
    r2k2=r2k2+(AiE*x(:,i,k)+ciE)'*(AiE*x(:,i,k)+ciE);
r3k2=r3k2+(AiI*x(:,i,k)+BiI*u(:,i,k)+ciI+siI(:,i,k))'*(AiI*x(:,i,k)+BiI
*u(:,i,k)+ciI+siI(:,i,k));
 r4k2=r4k2+min(lamdiI(:,i,k),siI(:,i,k))'*min(lamdiI(:,i,k),siI(:,i,k));
  end
    solvx=-inv([W(:,:,1)
A(1:1:lenAi_r,1:1:lenAi_c,1)';A(1:1:lenAi_r,1:1:lenAi_c,1)
B(1:lenBi_r,1:lenBi_c,1)])*[v(:,1);cn(1:lenCn,1)];
    xa(:,1)=solvx(1:nx);
    lenain(1)=length(solvx)-nx;
    ain(1:lenain(1),1)=solvx((nx+1):length(solvx));
   for i1=1:(n-1)
       air=-
(E1i(1:lenE1i_r(i1),1:lenE1i_c(i1),i1)*xa(:,i1)+e2i(1:lene2i_r(i1),1:le
ne2i_c(i1),i1));
       ait=phistore(1:lenphi_r(i1),1:lenphi_r(i1),i1)*[air'
ain(1:lenain(i1),i1)'];
       ait';
       ua(:,i1)=ait(1:nu);
       lenain(i1+1)=length(ait(:,1))-(nu+1+lenpib(i1)+1)+1;
```

```
ain(1:lenain(i1+1),i1+1)=ait((nu+1+lenpib(i1)+1):length(ait(:,1)));
       lenlamd(i1)=1+lenpib(i1);
       lamd(1:lenlamd(i1),i1)=ait((nu+1):(nu+lenlamd(i1)));
       xa(:,i1+1)=Ai*xa(:,i1)+Bi*ua(:,i1);
       lamdiEa(:,i1)=lamd(1,i1);
       lamdiba(1:lenpib(i1),i1)=lamd(2:lenlamd(i1),i1);
   end
   lamd(1:lenain(n),n)=ain(1:lenain(n),n);
   lenlamd(n)=1+lenpib(n);
   lamdiEa(:,n)=lamd(1,n);
   lamdiba(1:lenpib(n),n)=lamd(2:lenlamd(n),n);
   lamdiEa(:,:);
   lamdiba(:,:);
   rk=sqrt(r1k2+r2k2+r3k2+r4k2);
   if rk<theta
       f=-2;
       break;
   end
   for i0=1:n
     if i0==n
       siIa(:,i0)=-(AiI*(x(:,i0,k)+xa(:,i0))+ciIa(:,i0)+siI(:,i0,k));
       if lenmm2_r(i0)==0

lamdiIa(:,i0)=cof1(1:lenmm1_r(i0),1:lenmm1_c(i0),i0)*lamdiba(1:lenpib(i
0),i0);
         else
            if lenmm1_r(i0)==0

lamdiIa(:,i0)=cof2(1:lenmm2_r(i0),1:lenmm2_c(i0),i0)*AiI*xa(:,i0)+cof2(
1:lenmm2_r(i0),1:lenmm2_c(i0),i0)*ciIka(:,i0);
              else

lamdiIa(:,i0)=cof1(1:lenmm1_r(i0),1:lenmm1_c(i0),i0)*lamdiba(1:lenpib(i
0),i0)+cof2(1:lenmm2_r(i0),1:lenmm2_c(i0),i0)*AiI*xa(:,i0)+cof2(1:lenmm
2_r(i0),1:lenmm2_c(i0),i0)*ciIka(:,i0);
            end
         end
     else
       siIa(:,i0)=-
(AiI*(x(:,i0,k)+xa(:,i0))+BiI*(u(:,i0,k)+ua(:,i0))+ciIa(:,i0)+siI(:,i0,
k));
         if lenmm2_r(i0)==0

lamdiIa(:,i0)=cof1(1:lenmm1_r(i0),1:lenmm1_c(i0),i0)*lamdiba(1:lenpib(i
0),i0);
         else
            if lenmm1_r(i0)==0

lamdiIa(:,i0)=cof2(1:lenmm2_r(i0),1:lenmm2_c(i0),i0)*AiI*xa(:,i0)+cof2(
1:lenmm2_r(i0),1:lenmm2_c(i0),i0)*ciIka(:,i0)+cof2(1:lenmm2_r(i0),1:len
mm2_c(i0),i0)*BiI*ua(:,i0);
              else
```

```
lamdiIa(:,i0)=cof1(1:lenmm1_r(i0),1:lenmm1_c(i0),i0)*lamdiba(1:lenpib(i
0),i0)+cof2(1:lenmm2_r(i0),1:lenmm2_c(i0),i0)*AiI*xa(:,i0)+cof2(1:lenmm
2_r(i0),1:lenmm2_c(i0),i0)*ciIka(:,i0)+cof2(1:lenmm2_r(i0),1:lenmm2_c(i
0),i0)*BiI*ua(:,i0);
            end
         end
     end
   end

  if loop==1
      for j0=1:n
          lk((j0-1)*n_ieq+1:n_ieq*j0,1)=lamdiI(:,j0,k);
          sk((j0-1)*n_ieq+1:n_ieq*j0,1)=siI(:,j0,k);
          la((j0-1)*n_ieq+1:n_ieq*j0,1)=lamdiIa(:,j0);
          sa((j0-1)*n_ieq+1:n_ieq*j0,1)=siIa(:,j0);
      end
        aamax=1000000;
        for lt=1:(24*n_ieq)
            if la(lt,1)<0
               aa1=-lk(lt,1)/la(lt,1);
            end
            if sa(lt,1)<0
               aa2=-sk(lt,1)/sa(lt,1);
            end
            aa3=min(aa1,aa2);
            if aa3<aamax
                aamax=min(1,aa3);
            end
        end
        aa=aamax;

     for jj0=1:n
      for j0=1:n_ieq
          Lika(j0,j0,jj0)=lamdiIa(j0,jj0);
          Sika(j0,j0,jj0)=siIa(j0,jj0);
      end
     end
   miuk=0;
   miua=0;
   for k00=1:n
    miuk=miuk+lamdiI(:,k00,k)'*siI(:,k00,k)/n2;

miua=miua+(lamdiI(:,k00,k)+aa*lamdiIa(:,k00))'*(siI(:,k00,k)+aa*siIa(:,
k00))/n2;
   end
    zeta=(miua/miuk)^3;
  else
      for j0=1:n
          lk((j0-1)*n_ieq+1:n_ieq*j0,1)=lamdiI(:,j0,k);
          sk((j0-1)*n_ieq+1:n_ieq*j0,1)=siI(:,j0,k);
          lp((j0-1)*n_ieq+1:n_ieq*j0,1)=lamdiIa(:,j0);
          sp((j0-1)*n_ieq+1:n_ieq*j0,1)=siIa(:,j0);
```

```
      end
        aamax=1000000;
        for lt=1:(24*n_ieq)
            if lp(lt,1)<0
               aa1=-lk(lt,1)/lp(lt,1);
            end
            if sp(lt,1)<0
               aa2=-sk(lt,1)/sp(lt,1);
            end
            aa3=min(aa1,aa2);

            if aa3<aamax
                aamax=min(1,aa3);
            end
        end
        amax=aamax;
      k=k+1;
      a_mul=min(0.995*amax,1);
      x(:,1,k)=x(:,1,k-1)+a_mul*xa(:,1);
      for i0=1:n
          if i0==n
            lamdiI(:,i0,k)=lamdiI(:,i0,k-1)+a_mul*lamdiIa(:,i0);
            siI(:,i0,k)=siI(:,i0,k-1)+a_mul*siIa(:,i0);
            lamdiE(:,i0,k)=lamdiE(:,i0,k-1)+a_mul*lamdiEa(:,i0);
          else
             u(:,i0,k)=u(:,i0,k-1)+a_mul*ua(:,i0);
             x(:,i0+1,k)=Ai* x(:,i0,k)+Bi*u(:,i0,k);
            lamdiI(:,i0,k)=lamdiI(:,i0,k-1)+a_mul*lamdiIa(:,i0);
            siI(:,i0,k)=siI(:,i0,k-1)+a_mul*siIa(:,i0);
            lamdiE(:,i0,k)=lamdiE(:,i0,k-1)+a_mul*lamdiEa(:,i0);
          end
      end
  end
  end
    f=f+1;
   disp('Iteration Number'),k,
   disp('Convergence')
   Convergence_Parameter=rk/100000
   cog(k)=Convergence_Parameter;
      if f>100
        break;
     end
end

% %%%%%%%%%  PLOT  %%%%%%%%%
% subplot(2,2,1)
% hold on;
% grid on;
% axis([1 24 -30 60]);
% stairs(1:n,x(1,1:n,k),'y')
% stairs (1:n,x(2,1:n,k),'b')
% stairs (1:n,x(3,1:n,k),'g')
% stairs (1:n,x(4,1:n,k),'r')
```

```
% plot(1:n,Pwt,'*')
% plot(1:n,Pv,'o')
% legend('Fuel Cell','Microturbine','ESS')
% subplot(2,2,2)
% hold on;
% grid on;
% title('Battery Charging and Discharging')
% stairs (1:n,x(4,1:n,k),'r')
% subplot(2,2,3)
% hold on;
% title('State of Charge')
% bar(1:n,x(5,1:n,k))
% subplot(2,2,4)
% hold on;
% grid on;
% plot(1:k,cog(1:k),'b')
% title('Convergence Curve')
```

Appendix B

Modified Dynamic Programming

This part is used to calculate the set $(\tilde{z},\tilde{\zeta},\tilde{\lambda},\tilde{s})$.

In this procedure,

$$y_i^k = y_i + Q_i x_i^k + R_i u_i^k + A_{iE}^T \lambda_{iE}^k + A_{iI}^T \lambda_{iI}^k ,$$

$$z_i^k = z_i + R_i^T x_i^k + S_i u_i^k + B_{iE}^T \lambda_{iE}^k + B_{iI}^T \lambda_{iI}^k ,$$

$$c_{iE}^k = A_{iE} x_i^k + B_{iE} u_i^k + \hat{c}_{iE} ,$$

$$c_{iI}^k = A_{iI} x_i^k + B_{iI} u_i^k + \hat{c}_{iI} + s_{iI}^k + diag(\lambda_{iI}^k)^{-1} d_{ik} ,$$

$$G_i^k = diag(\lambda_{iI}^k)^{-1} diag(s_{iI}^k) .$$

The matrix G_i^k can be expressed as

$$G_i^k = \begin{bmatrix} P_{ib} & P_{if} \end{bmatrix} \begin{bmatrix} G_{ib} & 0 \\ 0 & G_{if} \end{bmatrix} \begin{bmatrix} P_{ib}^T \\ P_{if}^T \end{bmatrix},$$

where the diagonal elements in the second matrix on the right-side is sorted in ascending order. The number of columns in P_{ib} equals to the number of diagonal elements that less than one.

$$\bar{y}_i = y_i^k + A_{iI}^T \bar{P}_i c_{iI}^k , \quad \bar{z}_i = z_i^k + B_{iI}^T \bar{P}_i c_{iI}^k , \quad \bar{P}_i = P_{if} G_{if}^{-1} P_{if}^T ,$$

$$\bar{Q}_i = Q_i + A_{iI}^T \bar{P}_i A_{iI} , \quad \bar{R}_i = R_i + A_{iI}^T \bar{P}_i B_{iI} , \quad \bar{S}_i = S_i + B_{iI}^T \bar{P}_i B_{iI}$$

$$\bar{A}_i = \begin{bmatrix} A_{iE} \\ P_{ib}^T A_{iI} \end{bmatrix}, \quad \bar{B}_i = \begin{bmatrix} B_{iE} \\ P_{ib}^T B_{iI} \end{bmatrix}, \quad \bar{c}_i = \begin{bmatrix} c_{iE}^k \\ P_{ib}^T c_{iI}^k \end{bmatrix},$$

$$\bar{\lambda}_i = \begin{bmatrix} \bar{\lambda}_{iE} \\ \bar{\lambda}_{ib} \end{bmatrix}, \quad \bar{G}_i = \begin{bmatrix} 0 & 0 \\ 0 & G_{ib} \end{bmatrix},$$

$$\bar{\lambda}_{iI} = P_{ib}\,\bar{\lambda}_{ib} + P_{if}G_{if}^{-1}P_{if}^{T}(A_{iI}\,\bar{x}_i + B_{iI}\,\bar{u}_i + c_{iI}^{k}),$$

$$\bar{s}_{iI} = -[A_{iI}(x_i^k + \bar{x}_i) + B_{iI}(u_i^k + \bar{u}_i) + \hat{c}_{iI} + s_i^k].$$

Then,

$$H_{1i} = \bar{Q}_i + A_i^T W_{i+1} A_i,\ H_{2i} = \bar{R}_i + A_i^T W_{i+1} B_i,$$

$$H_{3i} = \bar{S}_i + B_i^T W_{i+1} B_i,$$

$$h_{4i} = \bar{y}_i + A_i^T v_{i+1},\ h_{5i} = \bar{z}_i + B_i^T v_{i+1},$$

$$F_{1i} = \begin{bmatrix} H_{3i} & \bar{B}_i^T & B_i^T A_{i+1,n}^T \\ \bar{B}_i & -\bar{G}_i & 0 \\ A_{i+1,n}B_i & 0 & B_{i+1,n} \end{bmatrix},$$

$$F_{2i} = \begin{bmatrix} H_{2i}^T \\ \bar{A}_i \\ A_{i+1,n}A_i \end{bmatrix},\ f_{3i} = \begin{bmatrix} h_{5i} \\ \bar{c}_i \\ c_{i+1,n} \end{bmatrix}.$$

The matrix F_{1i} is factored as

$$F_{1i} = \Phi_i \Sigma_i \Phi_i^T,$$

where Φ_i is an orthogonal matrix of eigenvectors and

$$\Sigma_i = diag(\sigma_1,....,\sigma_{nif}),\ \left|\sigma_j\right| \geq \left|\sigma_{j+1}\right|,\quad j = 1,....,n_{if} - 1.$$

Define

$$n_{ir} = \max(\max\{j \mid \left|\sigma_j / \sigma_1\right| \geq 1/c_{\max}\}, n_{if} - n),$$

$n_{in} = n_{if} - n_{ir}$, $c_{\max}$ is a positive scalar,

and

$\Sigma_{ir} = diag(\sigma_1,...,\sigma_{nir})$, $\Sigma_{in} = diag(\sigma_{nir+1},...,\sigma_{nif})$

$\Phi_i = [\Phi_{ir}, \Phi_{in}]$, $\Phi_{ir} \in R^{nif \times nir}$, $\Phi_{in} \in R^{nif \times nin}$.

The algorithm consists of four steps:

1) Calculate

$A_{Nn} = \bar{A}_N$, $B_{Nn} = -\bar{G}_N$, $c_{Nn} = \bar{c}_N$,

$v_N = \bar{y}_N$, $W_N = \bar{Q}_N$.

2) Calculate

$A_{in} = \Phi_{in}^T F_{2i}$, $B_{in} = \Sigma_{in}$, $c_{in} = \Phi_{in}^T f_{3i}$,

$W_i = H_{1i} - F_{2i}^T \Phi_{ir} E_{1i}$, $v_i = h_{4i} - F_{2i}^T \Phi_{ir} e_{2i}$,

Where

$E_{1i} = \Sigma_{ir}^{-1} \Phi_{ir}^T F_{2i}$, $e_{2i} = \Sigma_{ir}^{-1} \Phi_{ir}^T f_{3i}$, for *i=N-1,…,1.*

3) Solve the linear equation

$$\begin{bmatrix} W_1 & A_{1n}^T \\ A_{1n} & B_{1n} \end{bmatrix} \begin{bmatrix} \tilde{x}_1 \\ \tilde{a}_{1n} \end{bmatrix} = -\begin{bmatrix} v_1 \\ c_{1n} \end{bmatrix}.$$

4) Calculate

$\tilde{a}_{ir} = -(E_{1i} \tilde{x}_i + e_{2i})$, $\tilde{a}_{it} = \Phi_i \begin{bmatrix} \tilde{a}_{ir}^T, \tilde{a}_{in}^T \end{bmatrix}^T$,

$[\tilde{u}_i^T, \tilde{\lambda}_i^T, \tilde{a}_{i+1,n}^T] = \tilde{a}_{it}^T$, $\tilde{x}_{i+1} = A_i \tilde{x}_i + B_i \tilde{u}_i$,

for *i=1,…,N-1*, and set $\tilde{\lambda}_N = \tilde{a}_{Nn}$.

Appendix C

Hourly forecasted wind generation

Day-ahead forecasted wind generation (kw),

Hour	0:00	1:00	2:00	3:00	4:00	5:00	6:00	7:00	8:00	9:00	10:00	11:00
kw	5.46	4.01	4.01	3.51	4.68	4.94	7.14	7.16	6.36	5.72	6.89	5.85
Hour	12:00	13:00	14:00	15:00	16:00	17:00	18:00	19:00	20:00	21:00	22:00	23:00
kw	7.41	5.33	6.50	4.82	4.94	4.55	5.46	5.60	3.90	5.07	4.68	5.19

Actual wind generation (kw),

Hour	0:00	1:00	2:00	3:00	4:00	5:00	6:00	7:00	8:00	9:00	10:00	11:00
kw	6.14	4.36	4.15	3.90	4.54	5.11	7.45	7.09	6.64	5.46	6.58	6.17
Hour	12:00	13:00	14:00	15:00	16:00	17:00	18:00	19:00	20:00	21:00	22:00	23:00
kw	8.10	5.64	6.45	4.85	5.37	4.63	6.13	5.72	4.09	4.89	5.13	5.34

Wind generation forecasting (kw) for the next 24 hours at each hour.

hr / Time	1	2	3	4	5	6	7	8	9	10	11	12
0:00	4.86	4.91	3.84	5.50	5.72	7.34	7.30	6.96	6.87	7.29	6.55	7.68
1:00	4.98	3.80	5.80	5.35	7.38	7.46	7.10	6.28	7.31	6.85	8.11	5.98
2:00	4.19	5.24	4.95	7.54	7.35	7.31	6.09	7.52	6.05	8.13	5.64	7.28
3:00	4.81	6.09	7.15	8.08	7.34	6.76	6.99	6.33	7.72	6.29	7.01	5.91
4:00	5.42	7.23	7.44	6.51	5.94	7.17	6.35	7.47	6.41	7.63	5.40	5.52
5:00	7.83	7.23	6.64	6.14	7.87	5.87	7.46	5.53	7.27	5.69	5.71	5.09
6:00	7.74	6.88	6.25	7.25	6.46	8.02	6.31	7.45	5.59	5.39	5.52	6.10

7:00	6.63	5.92	7.16	6.37	7.78	6.43	7.01	5.04	6.02	5.72	5.99	5.73
8:00	5.82	7.20	6.81	7.45	6.44	7.37	5.40	5.63	4.83	6.01	6.75	4.56
9:00	7.00	6.16	7.81	6.14	6.66	5.68	5.06	5.33	6.05	6.53	4.76	6.15
10:00	6.82	8.10	5.54	6.78	5.88	4.97	5.13	5.66	6.77	4.76	5.67	5.25
11:00	8.58	6.10	7.46	5.36	5.45	5.54	5.56	5.75	4.11	5.54	5.68	6.15
12:00	5.77	6.73	5.40	5.34	5.69	6.56	5.66	4.79	5.39	5.19	5.85	6.59
13:00	6.53	5.49	5.99	5.35	5.69	6.04	4.45	6.25	4.87	6.22	6.23	4.46
14:00	5.80	6.11	5.42	5.87	6.30	4.03	6.16	5.74	6.17	5.77	4.72	4.03
15:00	5.02	4.93	6.10	6.38	4.39	6.05	5.54	6.35	6.10	4.40	4.13	4.24
16:00	5.31	6.61	5.88	4.71	5.42	5.49	6.02	5.54	4.31	4.27	4.31	5.69
17:00	5.85	6.54	4.47	5.11	4.89	6.06	6.03	4.19	4.41	4.24	4.91	5.82
18:00	6.37	4.71	5.83	5.81	5.44	6.31	4.29	4.15	4.24	5.22	5.49	7.93
19:00	4.28	5.21	5.81	5.96	6.04	4.77	4.66	4.29	5.33	5.80	7.77	8.35
20:00	5.30	4.85	6.03	5.57	4.64	4.64	4.54	5.26	5.41	7.95	8.04	6.98
21:00	5.50	6.03	5.99	4.03	4.40	4.02	5.00	5.17	8.13	7.67	7.43	6.18
22:00	6.11	5.66	5.04	5.19	4.13	5.74	5.64	7.33	7.39	6.85	6.61	7.88
23:00	6.48	4.68	5.12	4.35	5.38	5.91	8.19	8.34	6.36	6.75	7.62	7.04

hr / Time	13	14	15	16	17	18	19	20	21	22	23	24
0:00	6.23	6.80	5.42	5.77	5.61	6.61	6.25	4.07	5.25	4.99	6.20	5.77
1:00	7.60	5.16	5.84	5.45	5.92	6.28	3.99	5.13	5.32	6.13	6.58	4.16
2:00	5.64	5.83	5.09	5.56	5.87	5.00	5.25	5.67	5.84	6.66	4.10	4.54
3:00	5.15	4.86	5.63	5.76	4.94	5.77	5.34	5.36	6.48	4.75	4.43	4.13

4:00	4.95	6.54	6.04	4.03	6.01	5.15	5.48	5.94	4.12	4.16	4.64	5.83
5:00	6.12	5.95	4.79	5.30	5.50	5.41	5.90	4.76	4.94	3.61	5.80	5.87
6:00	6.02	5.03	6.12	5.34	5.94	6.16	4.25	4.37	4.08	4.96	5.95	7.37
7:00	4.21	5.56	5.39	5.50	6.18	4.86	4.27	3.65	5.04	5.32	7.65	7.76
8:00	5.70	4.96	5.78	6.21	4.82	4.48	3.95	5.87	4.98	8.20	8.25	7.32
9:00	5.75	5.59	6.30	4.24	4.04	4.40	5.28	5.51	8.23	7.89	7.10	6.75
10:00	5.26	6.28	4.06	4.09	4.14	4.80	5.92	8.12	8.02	6.54	6.51	7.51
11:00	5.53	4.48	4.64	4.01	5.47	5.69	7.49	7.67	6.38	6.90	7.09	5.98
12:00	4.51	5.18	3.87	5.52	5.73	7.79	7.99	7.16	5.93	7.04	7.05	7.62
13:00	4.23	4.02	5.26	5.08	7.85	7.43	6.82	6.41	7.19	6.20	8.15	5.64
14:00	4.02	5.06	5.13	7.35	7.66	6.47	6.43	7.45	6.69	8.25	6.09	6.54
15:00	5.61	5.44	7.25	7.47	6.54	6.05	7.41	6.48	7.96	6.38	7.12	5.95
16:00	5.35	8.08	7.97	6.37	6.44	7.35	6.95	7.41	5.88	7.00	5.37	5.86
17:00	7.43	8.26	6.68	6.63	7.11	6.19	7.52	6.02	7.32	5.47	5.45	5.32
18:00	8.08	6.78	6.51	7.38	6.86	8.41	5.63	7.23	5.51	5.58	5.59	5.78
19:00	6.62	5.84	7.02	5.93	7.90	5.86	6.93	5.73	5.69	5.47	6.58	6.76
20:00	6.13	7.06	6.55	7.72	5.38	7.40	5.11	5.47	5.37	5.89	6.48	4.37
21:00	7.81	6.33	8.38	6.23	6.95	5.07	5.88	5.68	5.85	6.40	4.43	6.07
22:00	6.80	7.79	5.97	6.60	4.95	5.10	5.36	6.05	5.82	4.49	5.25	4.75
23:00	8.04	5.90	7.46	5.09	5.53	5.63	6.15	6.61	4.79	5.77	4.98	5.99

REFERENCES

[1] http://www1.eere.energy.gov/femp/technologies/derchp_derbasics.html

[2] F. Katiraei, R. Iravani, N. Hatziaragyriou and A. Dimeas, "Microgrids management," *IEEE Power and Energy Magazine*, vol. 6, Iss.3, pp. 54-65, May-June 2008.

[3] F. A. Mohamed, "Microgrid modeling and online management," Ph.D dissertation, in department of Automation and Systems Technology, Helsinki University of Technology, 2008.

[4] C. Chen, S. Duan, T. Cai, B. Liu and G. Hu, "Smart energy management system for optimal microgrid economic operation," *IET Renew. Power Gener.*, vol. 5, Iss. 3, pp. 258-267, 2011.

[5] E. Sortomme and M. A. EI-Sharkawi, "Optimal power flow for system of microgrids with controllable loads and battery storage," *IEEE PES Power System Conf. and Exposition*, pp. 1-5, 2009.

[6] Bhuvaneswari Ramachandran, Sanjeev K. Srivastava, Chris S. Edrington, and David A. Cartes, "An intelligent auction scheme for smart grid market using a hybrid immune algorithm," *IEEE Trans. Industrial Electronics*, vol. 58, No. 10, October 2011.

[7] Xiaoping Liu, Ming Ding, Jianghong Han, Pingping Han and Yali Peng, "Dynamic economic dispatch for microgrids including battery energy storage," *IEEE International Symposium on Power Electron. for Distri. Gener. Sys.*, pp. 914-917, 2010.

[8] C. R. Dohrmann and R. D. Robinett, "Dynamic programming method for constrained discrete-time optimal control," *Journal of Optimization Theory and Applications*, vol. 101, No. 2, pp. 259-283, May 1999.

[9] Rush D. Robinett, David G. Wilson, G. Richard Eisler and John E. Hurtado, "Applied dynamic programming for optimization of dynamical systems," Advance in Design and Control, SIAM, 2005.

[10] Texas Instruments Europe, "Field oriented control of 3-phase Ac-motors," Literature Number BPRA073, February, 1998.

[11] 568000 DSP Manual (2007), "3-Phase AC Induction Vector Control Drive with Single Shunt Current Sensing," Freescale, p. 25, incl. esp. eq. 2-37, Retrieved May 16, 2012.

[12] W. Musial, S. Butterfield and B. McNiff, "Improving wind turbine gearbox reliablity," *European Wind Energy Conference*, Milan, Italy, May 7-10, 2007.

[13] R. Chedid, H. Akiki, and S. Rahman. A decision support technique for the design of hybrid solar- wind power systems. *IEEE Transaction on Energy Conversion*, pg. 76– 83, March 1998.

[14] http://amrita.vlab.co.in/?sub=1&brch=195&sim=360&cnt=1

[15] H. Patel and V. Agarwal, "MATLAB-Based modeling to study the effects of partial shading on PV array characteristics," *IEEE Transaction on Energy Conversion*, vol. 23, iss. 1, pg. 302-310, 2008.

[16] R. Mukund. Wind and solar power systems. CRC Press, CRC Press LLC, 2000 N.W., Corporate Blvd., Boca Raton, Florida 33431, 1999.

[17] M. J. Moore, "Micro-turbine generators," Professional Engineering Publishing, Bury St. Edmunds and London, UK, 2002.

[18] S. Haugwitz, "Modeling of microturbine systems," Master's thesis, Department of Automatic Control, Lund Institute of Technology, Lund, Sweden, May 2002.

[19] R. Lasseter, "Dynamic models for micro-turbines and fuel cells," *IEEE Power Engineering Society Summer Meeting,* volume 2, 761 – 766, British Columbia, Canada, July 2001. NREL Report No. SR-560-32527.

[20] George Wand, "Fuel Cells History, part 1," Johnson Matthey plc., p. 14, Retrieved in Oct. 2008.

[21] "Roger Billings Biography", International Association for Hydrogen Energy, Retrieved 2011-03-08.

[22] A. M. Azmy and I. Erlich, "Online optimal management of pem fuel cells using neural networks," *IEEE Transactions on Power Delivery*, vol.20, iss. 2, pg. 1051 – 1058, April 2005.

[23] E. Bakhoum, "New mega-farad ultracapacitors," *IEEE Transaction on Ultrasonics,* vol. 56, iss. 1, pg. 14-21, 2009.

[24] R. Hebner, J. Beno and A. Walls, "Flywheel batteries come around again," *IEEE Spetrum,* vol. 29, iss. 4, pg. 46-51, 2002.

[25] S. Barsali and M. Ceraolo, "Dynamical models of lead-acid batteries: implementation issues," *IEEE Transaction on Energy Conversion*, vol. 17, iss. 1, pg. 16-23, 2002.

[26] Z. M. Salameh, M. A. Casacca and W. A. Lynch, "A mathematical model for lead-acid batteries," *IEEE Transaction on Energy Conversion*, vol. 7, iss. 1, pg. 93-98, 1992.

[27] Alberto Borghetti, Mauro Bosetti and Samuele Grillo, "Short-term scheduling and control of active distribution systems with high penetration of renewable resources," *IEEE Systems Journa*l, vol. 4, No. 3, September, 2010.

[28] Antonis G. Tsikalakis and Nikos D. Hatziargyriou, "Centralized control for optimizing microgrids operation," *IEEE Trans. Energy Conversation*, vol. 23, No.1, March, 2008.

[29] D. P. Bertsekas, Dynamic Programming and Optimal Control, 3rd edition, Athena Scientific, Belmont, 2005.

[30] Nuno P. Faisca, Konstantinos I. Kouramas, Pedro M. Saraiva, Berc Rustem and Efstratios N. Pistikopoulos, "A multi-parametric programming approach for constrained dynamic programming problems, " *Optimization Letters*, Jan., 2007.

[31] Stavros Papathanassiou, Nikos Hatziargyriou, Kai Strunz, “A benchmark low voltage microgrid network,” *CIGRE Symposium*, Athens, April 13-16, 2005.

[32] V. Svoboda, 2004, "WP3.1 Define performance requirements for energy storage systems in each category," Center for Solar Energy and Hydrogen Research, Baden-Württemberg, 2004.

[33] S. Drouilhet, B.L. Johnson, "A Battery Life Prediction Method for Hybrid Power Applications," AIAA Aerospace Sciences Meeting and Exhibit, 1997.

[34] Henrik Bindner, Tom Cronin, Per Lundsager, James F. Manwell, Utama Abdulwahid and Ian Baring-Gould, "Lifetime modeling of lead acid batteries," Riso National Laboratory, Roskilde, Denmark, April 2005.

[35] Susan M. Schoenung and Willam V. Hassenzahl, "A life-cycle cost study," Sandia National Laboratories, 2003.

[36] P. Symons, "Life estimation of lead-acid battery cells for utility energy storage," *Proceedings of the Fifth Conference on Batteries for Utility Storage*, San Juan, Puerto Rico, July, 1995.

[37] Shu Fan, J.R. Liao, R. Yokoyama, Luonan Chen and Wei-Jen Lee, "Forecasting the wind generation using a two-stage network based on meteorological information," *IEEE Transaction on Energy Conversion*, vol. 24, iss. 2, pg. 474-482, 2009.

[38] Y. V. Makarov, P. V. Etingov, Jian Ma, Zhenyu Huang and K. Subbarao, "Incorporating uncertainty of wind power generation forecast into power system operation, dispatch, and unit commitment procedures," *IEEE Transaction on Sustainable Energy*, vol. 2, iss. 4, pg. 433-442, 2011.

[39] Jie Shi, Wei-Jen Lee, Yongqian Liu, Yongping Yang and Peng Wang, "Forecasting power output of photovoltaic systems based on weather classification and support vector machines," *IEEE Transaction on Industry Applications*, vol. 48, iss. 3, pg. 1064-1069, 2012.

[40] E. Lorenz, J. Hurka, D. Heinemann and H. G. Beyer, "Irradiance forecasting for the power prediction of grid-connected photovoltaic systems," *IEEE Journal of*

Selected Topics in Applied Earth Observations and Remote Sensing, vol. 2, iss. 1, pg. 2-10, 2009.

[41] http://graphical.weather.gov/

[42] http://www.accuweather.com/